NRL REPORT 4043

SIDE-LOBE CONFERENCE

under the auspices of the
Radio Divisions I and II

28 April 1952

NAVAL RESEARCH LABORATORY

WASHINGTON, D.C.

SIDE-LOBE CONFERENCE

under the auspices of the
Radio Divisions I and II

28 April 1952

NAVAL RESEARCH LABORATORY

WASHINGTON, D.C.

FOREWORD

This side-lobe conference was an outgrowth of the Fourth Symposium on Scanning Antennas. Several papers offered for presentation at the Symposium appeared to convey information on the general subject of side-lobe evaluation and suppression. It was therefore felt advisable to include these papers in a separate session and to invite additional papers to fill out the program.

The subject of this conference, the side-lobe problem, will always be present in the microwave antenna field, since any reduction in side-lobe level will be followed by requests from the systems engineers for yet further reduction in these levels. The mechanically perfect objective, with fixed feed at the focus, will always have diffraction lobes of a level which will be too high for some system applications. Deviations from a perfect objective or a repositioning of the feed will introduce errors whose first effect is to increase the side-lobe level. For a particular antenna, the diffraction lobes and the effects of these errors present the designer with a very complex problem. It is necessary that he determine the origin of the pattern lobes and devise some means for maintaining their intensity below a certain specified level.

The origin of the side lobes might be considered the subject of most of the papers published in this report. Two of the papers consider the general problem of relating the pattern characteristics, one of which is side-lobe level, to the aperture illumination. Two other papers consider the effect on the pattern of mechanical errors in the paraboloid reflector which is used as the focusing objective. The remaining paper describes a method of reducing the side lobes caused by diffraction. All of these papers provided definite contributions toward solution of the side-lobe problem; it is evident that further work will be done in evaluating particular aperture distributions and in developing methods of side-lobe suppression.

Thanks are extended to Dr. R. J. Adams for his work as Chairman of this Conference.

CONTENTS

A Method of Side-Lobe Reduction

Carlyle J. Sletten and William G. Mavroides
Air Force Cambridge Research Center

INTRODUCTION

Whenever narrow beamwidth and high gain are required, antennas with large apertures are needed. This usually means a reflector or lens in the antenna system. The designer would like to exercise what control he can over the shape of the antenna patterns. He is limited, however, by some fundamental restrictions, but the method of analysis he uses should give him maximum flexibility within these fundamental limits.

There are several analytic methods of studying antenna performance. We have borrowed two tools (geometric and physical optics) from an earlier science in order to get a connected theory of antenna behavior which will verify experimental data. These tools can be used in two basically different ways. First, we can treat the antenna as a transmitting antenna. We place a point source with some assumed directivity, in the focal region of the lens or reflector; and by the use of geometric optics we trace the rays to some aperture plane. Pattern control is obtained by controlling the directivity of the point source—that is, tapering the illumination on the aperture. Then we use physical or Fraunhofer optics to compute the far field by the use of amplitude and phase distribution across the aperture. This is a useful and well-accepted procedure.

A second method is to consider the antenna as a receiving antenna. This analysis consists of considering the field distribution set up in the focal region when a plane wave is incident on the reflector or lens. Now it is not so easy to separate geometric optics from physical optics. We can use geometric optics to find the power and phase distribution, neglecting diffraction effects. This was done at our laboratory in the case of the spherical reflector (1), and recently the same was done in the case of the paraboloid. However, superimposed on the field distribution predicted by geometric optics are the bunching or quantizing effects of physical optics. This paper describes how the focal-field distributions caused by diffraction can be coped with experimentally. It does not handle the complex mathematics needed to compute focal fields to high approximation (2,3). We do not claim that treating a reflector or lens as a receiving antenna is superior to the established procedure of viewing the design entirely as a transmitting problem. But we have found the receiving-antenna approach useful in that it suggests the form of primary feed needed in the focal region to produce a given pattern. The method of amplitude-taper control fails to suggest remedies in the cases where there are optical aberrations.

THE UNDERLYING IDEA

Is the reduction of illumination on the edge of the aperture the only effective method of controlling side-lobe level? Encouraged (1) with our success in the use of multiple sources for correcting geometric optical errors, it was only natural to apply such techniques to the physical optics problem of reducing diffraction lobes.

As with the geometric optics problem, we think of our antenna as a receiving collima A plane wave incident on the lens aperture excites a concentrated field distribution in the focal region. This field distribution is known as the Airy disc structure. There comes t mind the idea of constructing a primary feed tailored to accept from one direction only a the power from the rings. This is not so hard to do once we know the spatial distributio phase, and polarization of the fields in the Airy discs. With the absorbers thus arrayed i space, we might choose to reduce side lobes rather than to obtain maximum gain. This was done by manipulating the phase and degree of coupling from the various rings.

This selective absorption (or by reciprocity, transmission) obtained by separating th primary feed into several apertures with control over the phase and amplitude of the com bined powers suggests that considerably more variation in pattern characteristics can be had with a compact primary feed than was possible with the taper-control technique. The conclusions are implied in some of the amplitude and phase comparison schemes propose in late years. This is speculative since I know of no coherent mathematical theory embra ing the whole subject of antenna potentialities.

PATTERN CHARACTERISTIC LIMITATION

By selecting power from different locations in the focal region and combining it in one transmission line, the resultant pattern can be modified within certain limits. These limiting conditions on antenna patterns have not, in general, been rigorously set forth. When a given aperture and wavelength is used, the beamwidth in all probability cannot be made much smaller than that which is obtained by the use of a "point source" as the prim feed. Ruze (4) has shown that side lobes cannot be reduced indefinitely low on any physic realizable system. There also exist some basic functional relations (5) between resolutic (beamwidth) and contrast (side-lobe level) which makes it difficult to improve one without sacrificing the other.

FIELDS IN FOCAL REGION

The situation in the focal region is roughly sketched in Figures 1 and 2. The field distribution is independent of the type of pickup used, however, it is closely related to the polar plot or antenna pattern measured with a small horn. The important features of foca distribution are: (1) The spacing of the rings and power distribution can be approximate simply, once the wavelength aperture size and focal length are known (see Appendix); (2) the field in any disc is nearly uniform in phase, and the phase changes about 180 degrees from disc to disc; and (3) with an incident plane-polarized wave the polarization in the disc structure is not usually homogenous.

A knowledge of the field structure in the focal region is needed only to determine the approximate configuration and phasing of the small radiators; final adjustments can be made by pattern measurements.

THE PROCEDURE AS APPLIED TO A SPHERICAL REFLECTOR

The technique is best explained by an actual example. When a spherical reflector is fed by a small horn, symmetric diffraction patterns which show evidence of spherical aberration are obtained. By moving along a radius, patterns with highest gain and lowest side lobes are found inside the geometric focus R/2 (6). However, a side lobe level of about 13 db is the best that can be realized. Because of phase errors and shadowing, increasing the horn size does not reduce the side lobes. This point has been diligently checked.

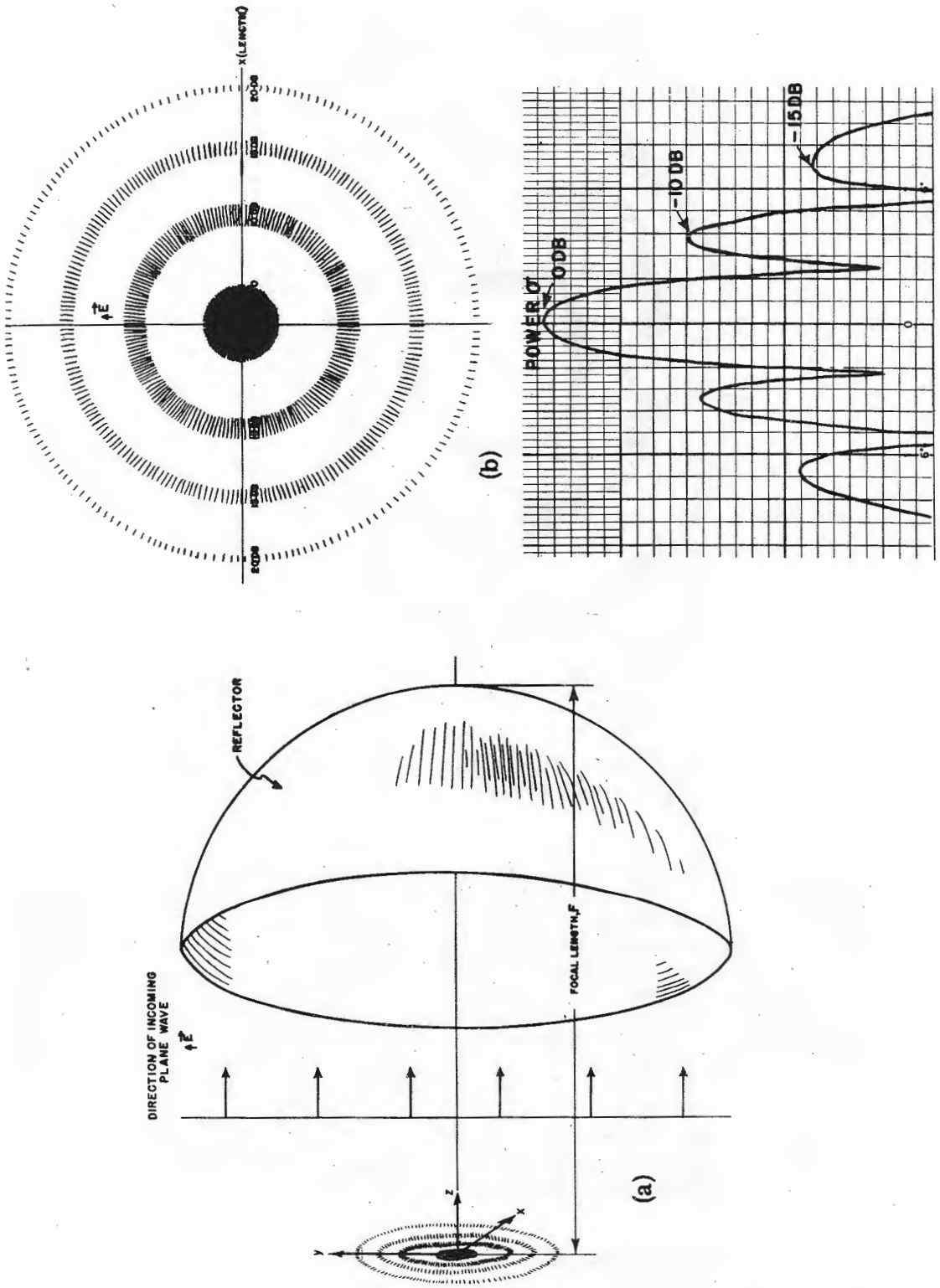

Figure 1 - Sketch illustrating power density in focal region of a reflector

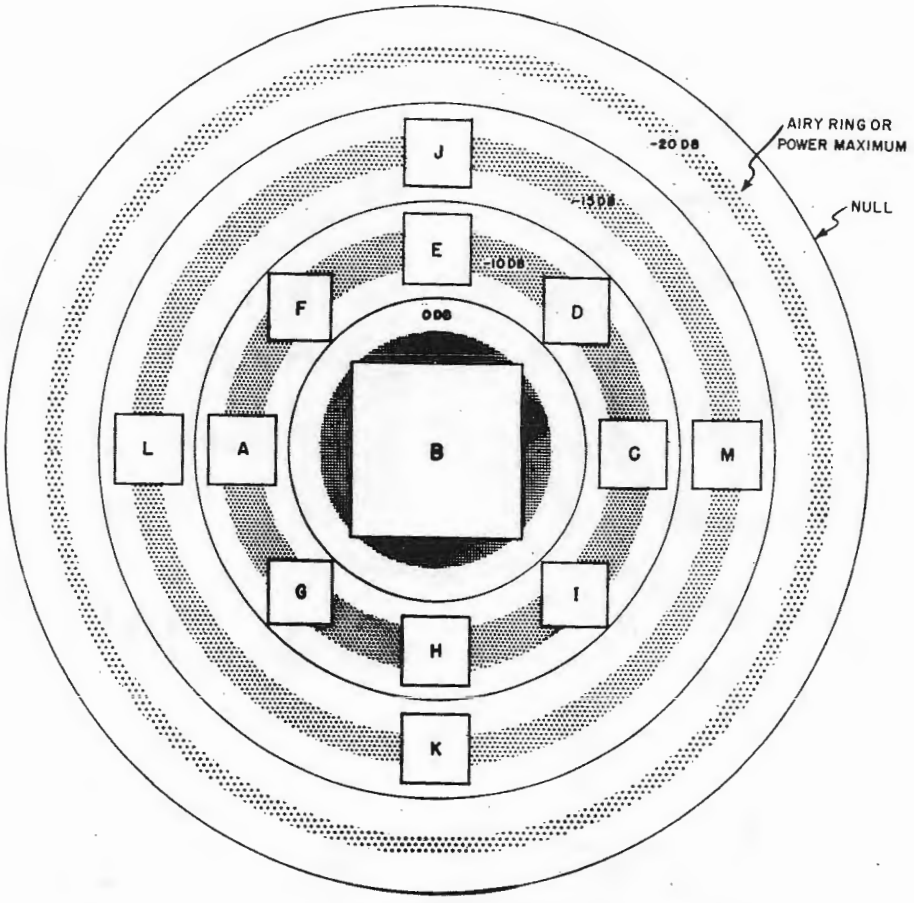

Figure 2 - Illustration of how horns might be arranged in the focal region for side-lobe reduction

An optimum position is found, and a pattern is taken with one horn first; then another horn is placed beside it about one inch away (X-band). The pattern of the second horn will be the same as that obtained with the first horn only it will be displaced in angle such that the first side lobe of its pattern occurs directly under the main lobe of the first horn (see Figure 3). As this is a symmetric situation, the same result is obtained by placing a horn on the other side of the first feed. The next step is to reduce the gain of the two side horns until they have a power level in their main beam equal to the side-lobe level of the center feed. As stated before, the phase throughout the lobes is nearly uniform. All we must do is mix these three signals in the proper phase, and the resultant pattern should have much lower side lobes. This can be done by properly tuning two magic tees as sketched in Figure 4.

Three independent input terminals are available with attenuators and phase shifters in each arm; thus the signals may be mixed. You will note that the side lobes on one side can be cancelled without affecting the other lobes, and we can proceed stepwise to the result we want.

There are several favorable conditions here. One is that on a scanning sphere the F/D is usually 1/2; this means that aperture spacing of about 1 inch will hold for all radius spheres at X-band. The side lobes are nearly as wide as the main beam, and this aids complete cancellation. The second side lobe is about 10 db down from the first lobe; therefore there is a tendency to reduce the second side lobe also.

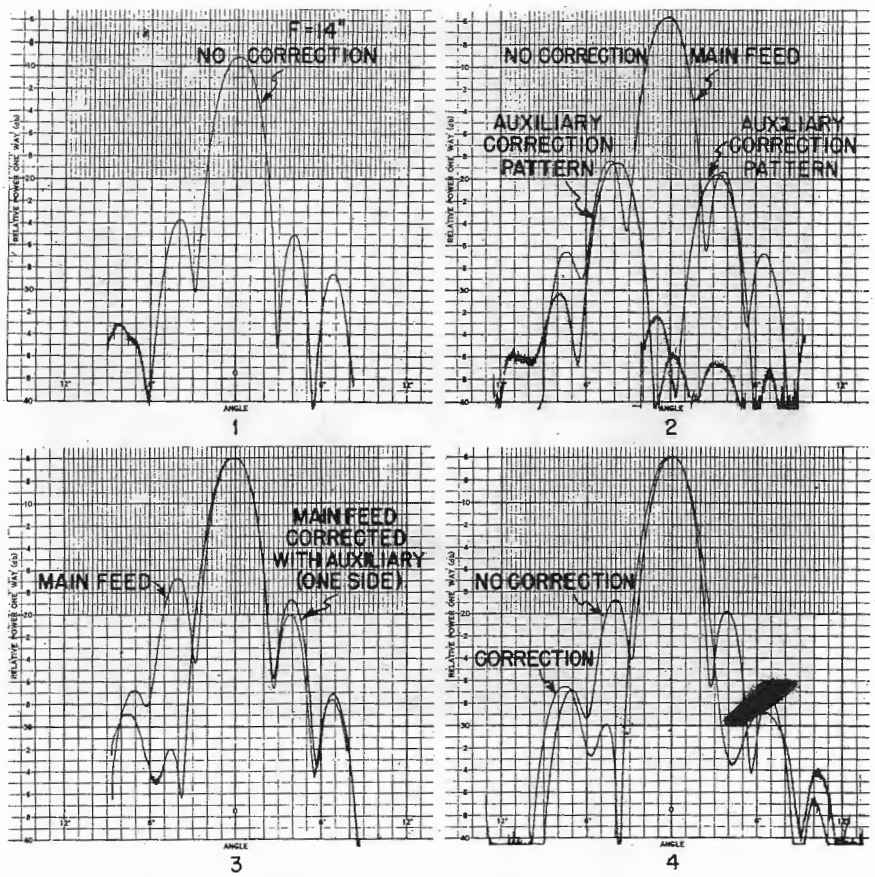

Figure 3 - Sequence showing correction process

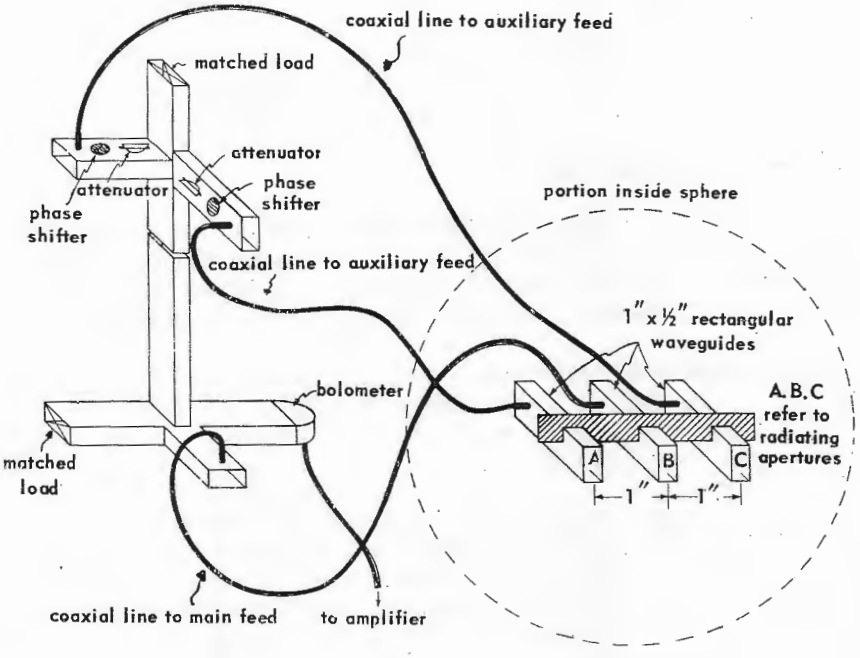

Figure 4 - Magic-tee mixer used to correct E-plane patterns on sphere

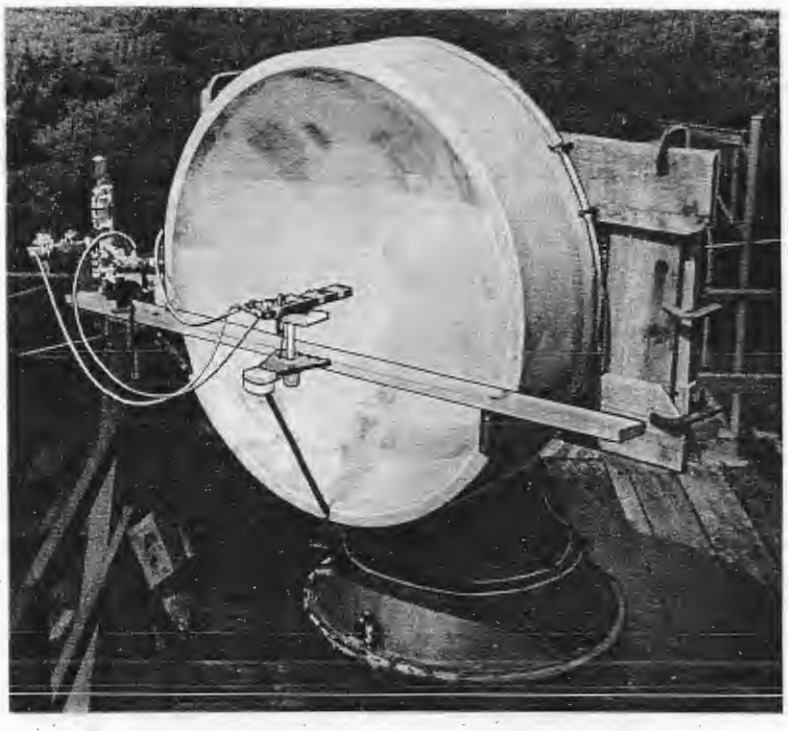

Figure 5 - Three-element primary feed mounted on spherical reflector

We have succeeded in reducing the side lobes on a spherical reflector where the taper control method fails. Figure 5 is a photograph of the experimental arrangement. This method should also succeed on a lens or paraboloid. It can be demonstrated analytically by summing

$$A_i \frac{\sin(\theta - \theta_i)}{(\theta - \theta_i)} \text{ functions.}$$

COMPARISON OF COUPLING DEVICES

Now that this method is demonstrated workable, we naturally think in terms of applications. A more efficient method of mixing or coupling the signal must be found, since the magic tees lose one-half the main-lobe power in a matched load. Our studies have been restricted to two couplers: E-plane septums and 2-hole directional couplers.

The E-plane septums are easily analyzed approximately. It essentially divides power without phase shift. As there is no absorption of power at the junctions; all energy must go out the arms. Figure 6(a) shows such a double septum tee. It was found difficult to make, and very sensitive to adjust.

The directional coupler is easier to design, but for the purpose at hand it has one bad feature: It introduces a 90-degree phase shift between arms. This shift is a lead or lag, depending on whether an E- or H-coupler is used. One is usually trying to bring the energy from the auxiliary guides into phase with that in the main guide so that there will be minimum phase error. There are two means of obtaining this phase correction. First, the polystyrene dipper type of corrector may be used for phase delay; second, metal insert

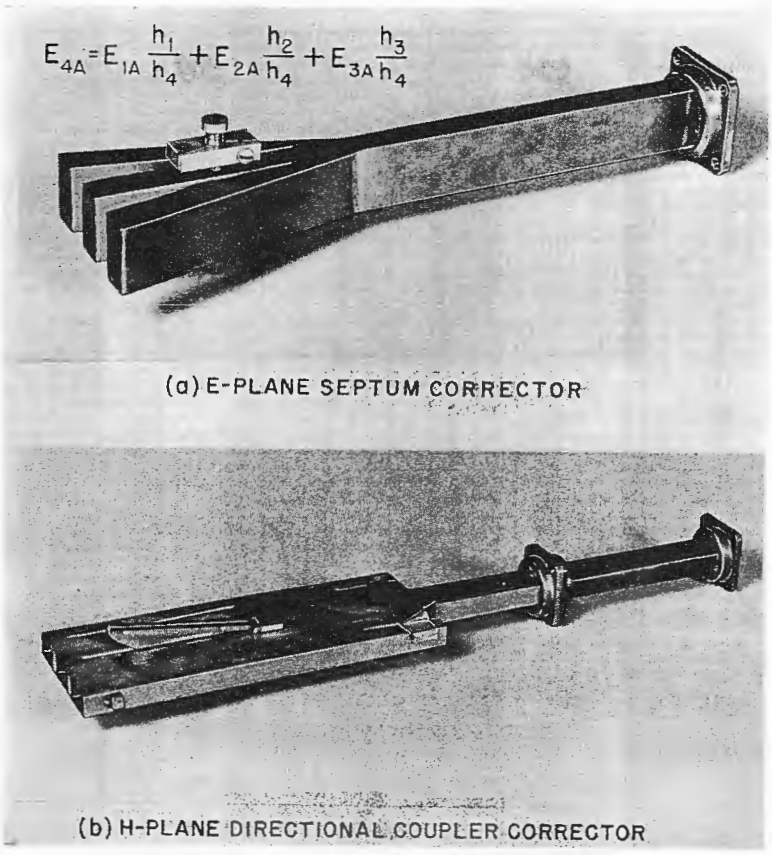

Figure 6 - E- and H-plane correcting feeds

which narrow the waveguide walls may be used to advance the phase. Figure 6(b) shows a model using the dipper type. A typical pattern obtained from this model is shown in Figure 7.

It was found that triple-horn side-lobe reduction is not critical to frequency or focusing changes.

PRACTICAL APPLICATIONS

The Airy discs on a sphere are circular; it is hard to build a good circular structure with rectangular guide. A row of three horns will reduce side lobes to 22 db in the plane containing the horns and planes rotated 30 degrees will have side lobes less than 18 db. However, correction in the two principal planes is not sufficient to produce good patterns in the diagonal planes. Figure 8 shows an attempt to correct the sphere simultaneously in all planes. The principal planes can be simultaneously corrected, but the diagonal planes show little correction.

A readier application is found in a pillbox scanner as described by W. Rotman. Only three apertures, coupled as in Figure 6(a), are needed to make a correction feed for this single-plane problem. We plan to try out the two-layer pillbox using this correction technique, but the work has not been completed.

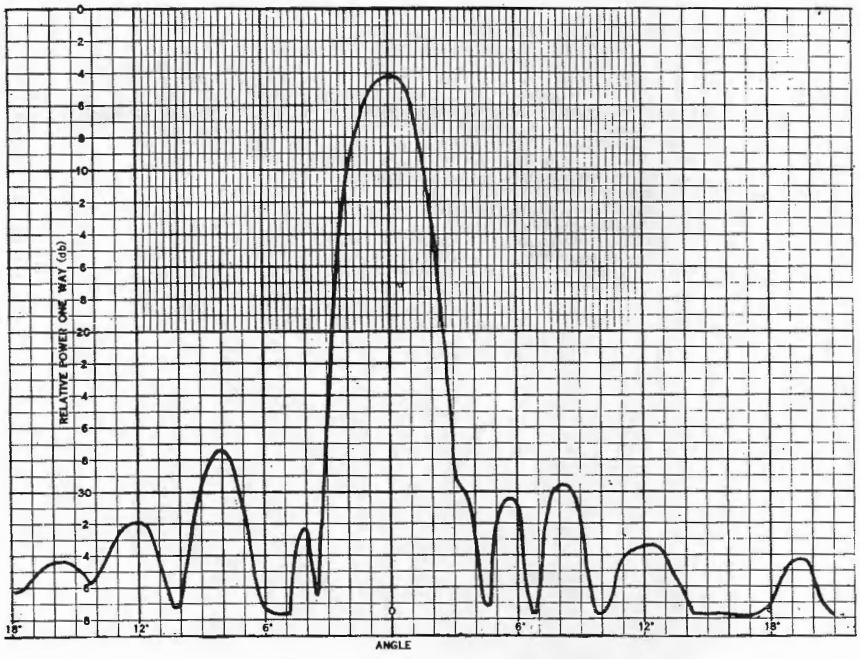

Figure 7 - H-plane pattern obtained by the use of a directional-coupler three-element feed

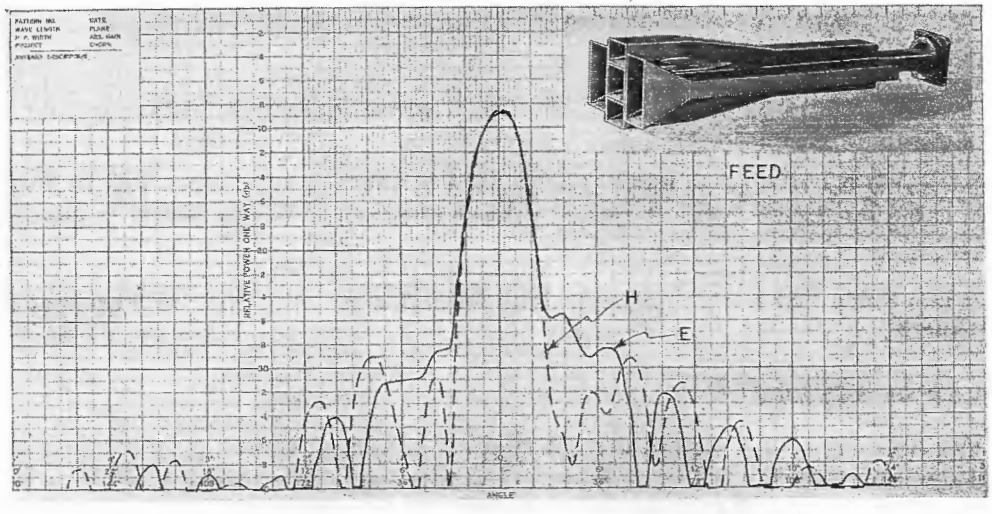

Figure 8 - E- and H-plane corrector for a spherical reflector, and the resulting patterns obtained

SUMMARY

We have evidence that side lobes can be reduced by coupling together small apertures in the focal region, and a technique has been outlined for side-lobe reduction on a spherical reflector or on a circular cylinder. Different coupling components have been successfully shown to achieve this pattern control. This method of side-lobe control should warrant consideration of a circular pillbox scanner.

It is suggested that more efficient side-lobe control can be had by tailoring the primary feed configuration to the field focal structure of the lens or reflector. Side lobes are a low-power feature of the pattern, and they can be cancelled by low-power couplers. Optical aberrations can be corrected by distributed radiators, usually arrayed longitudinally to the axis. This paper asserts that physical optical effects can be modified, subject to certain limitations—even in the presence of optical errors, by a transverse distribution of radiators.

ACKNOWLEDGMENTS

Most of the results listed in this paper were obtained with the enthusiastic assistance of William Mavroides and Richard Mack. The shop work was done by J. Lyons and J. Andriotakis, under the supervision of J. R. Baker. My Laboratory Chief, R. C. Spencer, and Section Chief, R. Hiatt, both supplied many helpful and encouraging ideas.

APPENDIX
Spatial Relation of Airy Rings

Because of the symmetry of the sphere (or circular cylinder) a point feed, fixed with reference to the reflector, will generate the same pattern when the system is rotated as will be obtained by leaving the reflector fixed and rotating only the feed about the center of the sphere. This is due to the wide-angle behavior of a spherical reflector. This situation is illustrated in Figure A1. If α_1 is the angle of the first side lobe in the pattern taken by rotating the reflector and feed in a plane wave, then the distance $x = L \tan \alpha_1$.

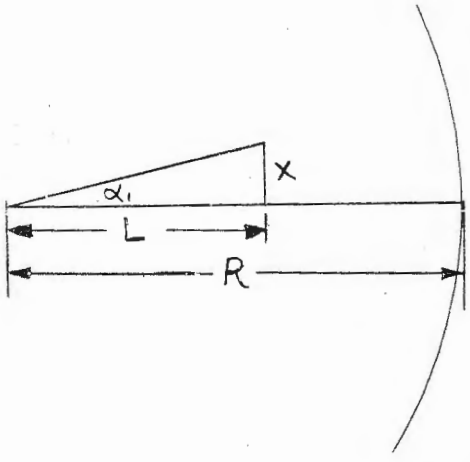

Figure A1 - Spherical reflector with point feed

Computation of the focal fields by integrating all the currents on the spherical reflector has been attempted by J. Walsh of this laboratory, but the analytic difficulties were tremendous. The polarization components according to geometric optics are as shown in Figure A2. Assume a plane wave e^{-jkz} moving in the positive z direction along a radius of the spherical reflector $x^2 + y^2 + z^2 = 1$. Using equation 32c page 140 of Reference 9,

$$\vec{E}_{\text{reflected}} = (\hat{n} \cdot \vec{E}_i)\hat{n} - (\hat{n} \times \vec{E}_i) \times \hat{n}$$

$$\hat{n} = x\hat{i} + y\hat{j} + z\hat{k}$$

$$x = \sin\psi \cos\theta, \quad y = \sin\psi \sin\theta, \quad z = \cos\psi$$

$$\text{Let } \vec{E}_i = \hat{j}$$

$$\vec{E}_r = 2xy\hat{i} + (y^2 - x^2 - z^2)\hat{j} + 2zy\hat{k}$$

$$\vec{E}_r = 2\sin^2\psi\cos\theta \sin\theta\hat{i} + (\sin^2\psi\sin^2\theta - \sin^2\psi\cos^2\theta - \cos^2\psi)\hat{j} + 2\sin\psi \sin\theta \cos\psi\hat{k}.$$

Using geometric optics we can assume that along the line $x = 0$, $y = 0$

$$\sec\psi = 1/2 + z$$

$$1/2 \leqslant z \leqslant 1.$$

Depending on the illumination, we can integrate in θ and find the polarization components as a function of ψ (or Z) along the z axis. Much can be inferred qualitatively about the polarization of focal fields by this analysis. We have checked and found that these polarizations are strongly present. No attempt to tailor a feed to accommodate them has been made.

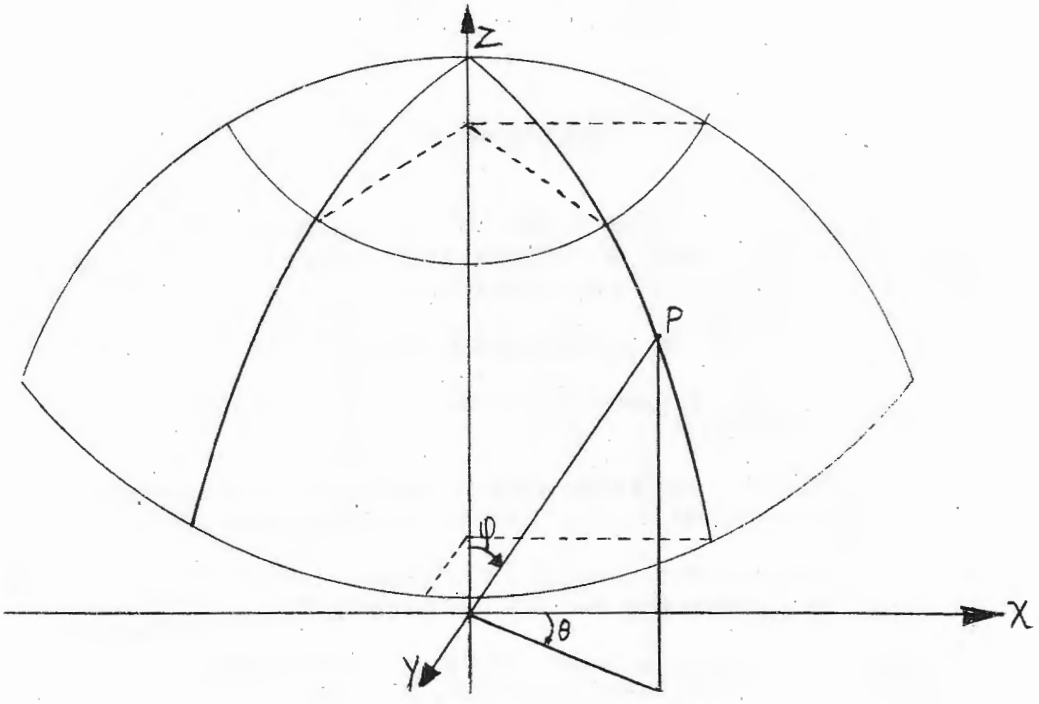

Figure A2 - Spherical coordinate system

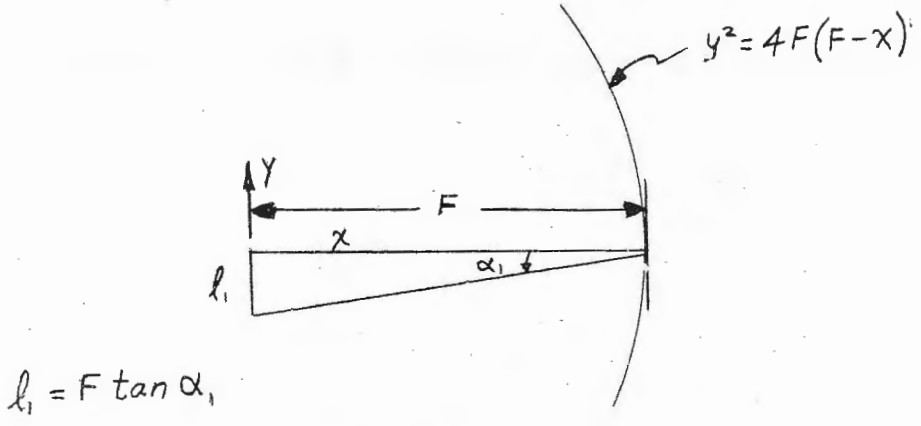

Figure A3 - Geometry of paraboloid for small α_1

On a paraboloid the geometry for small α_1 is approximately as shown in Figure A3. The angular coordinate α_1 of a side lobe is measured from the pattern or computed from functions of

$$\frac{\sin x}{x}$$ (see Reference 8).

* * *

REFERENCES

1. Spencer, R. C., Sletten, C. J., and Walsh, J. E., "Correction of Spherical Aberration by a Phased Line Source," Proc. of the National Electronics Conference, Vol. 5, Chicago, Ill. (1950) Also - AFCRC Report E5069, May 1951

2. Zunike, F., and Nyboer, B. R. A., Editions de la Revue d'Optique (1949) 227

3. Zucker, Francis J., "The Behavior of Microwaves in Focal Regions," presented at New York IRE, March 1951

4. Ruze, John, "Effect of Aperture Distribution Errors on the Radiation Pattern," AF Cambridge Research Center, Antenna Lab. Memorandum, January 1952

5. Dolph, C. L., "A Current Distribution for Broadside Arrays Which Optimizes the Relationship Between Beamwidth and Side-Lobe Level," Proc. IRE 34, 335 (1946)

6. Spencer, R. C., "Theoretical Analysis of the Effect of Spherical Aberration on Gain," AF Cambridge Research Center Report E5082, Dec. 1951

7. Rotman, Walter, "A Rapid-Scan Circularly Symmetrical Pillbox Antenna," presented at IRE Convention, New York, March 1952

8. Bell Lab. Staff, Radar Systems and Components, L. Van Nostrand, 1949. See page 780 ff.

9. Silver, S., Microwave Antenna Theory and Design, Rad. Lab. Series, Vol. 12, McGraw-Hill, 1949

* * *

EFFECT OF APERTURE DISTRIBUTION ERRORS ON THE RADIATION PATTERN

John Ruze
Air Force Cambridge Research Center

INTRODUCTION

The side lobes of a radiation pattern may be effectively suppressed by tapering the aperture distribution. In particular, Dolph[1] has shown that for discrete elements the properties of the Tschebyscheff polynomials may be utilized to obtain any degree of side-lobe suppression; furthermore, this distribution has certain optimum characteristics. Similar techniques are adaptable to a continuous aperture.

Theoretically, therefore, the side-lobe level may be chosen as low as desired. This paper treats the effect of unavoidable errors which occur when the antenna is constructed. A little consideration indicates that slight deviations from the theoretical current distribution may cause profound changes in the side-lobe level and, in general, a reduction in gain. This becomes clear when we consider the vector addition of the contributions from the various antenna elements. In the side-lobe region we require almost complete interference, and the vector magnitudes must be chosen so that the cancellation is within our tolerance over the entire region. We suspect that as the permitted side-lobe level is decreased the aperture distribution must be maintained even more precisely to realize this destructive property more completely. The engineering question naturally arises: To what precision must the distribution be maintained for a given side-lobe level, and, conversely, what side lobes are caused by given antenna errors?

NATURE OF APERTURE ERRORS

The aperture distribution errors may be of two types:

(a) what we call predictable errors and

(b) random errors.

Predictable errors are those which occur because of the omission of some factor in the design or engineering analysis. In this classification we would include errors caused by such factors as (a) mutual impedance between elements, (b) diffraction at a lens antenna step, (c) termination mismatch of a broadside or slot array, and (d) fixed error due to machining or faulty r-f measurements.

In contrast, random errors are caused by slight accidental deviations of the system parameters from their design value. Examples of such random errors are (a) machining errors in a broadside or slot array (these may cause an error in the current delivered to an element or actually radiated from it), (b) r-f measurement errors incurred in adjusting

[1] Dolph, C. L., "A Current Distribution for Broadside Arrays which Optimizes the Relationship between Beamwidth and Side-Lobe Levels," Proc. Inst. Radio Engrs., 34:335 (June 1946)

the array, (c) wall-spacing errors in metal-plate lenses, and (d) random distortion of the surface of a parabolic mirror.

In a constructed antenna it may be difficult to differentiate the two classes of errors. However, they can always be theoretically resolved, for if we designate the desired aperture distribution as $f_0(x)$, the distribution of a given antenna as $f(x)$, and the system average distribution (i.e., the average distribution of a large number of similar antennas) as $\overline{f(x)}$, then the predictable error is given by

$$\overline{f(x)} - f_0(x)$$

and the random error by

$$f(x) - \overline{f(x)}.$$

Predictable errors, once known or measured, may be treated by standard methods and have been discussed in the literature.[2] Their effect on the radiation pattern is characterized by strong side lobes in some "preferred" direction. Random errors, due to their nature, form a statistical problem. We can speak only about what happens on an "average" over a large number of "seemingly" identical antennas and how the probability of a given side-lobe magnitude varies from this system average. This paper will deal only with the random type of error. The next section serves as a statistical introduction.

STATISTICAL INTRODUCTION[3]

Let us consider the sum "S" of a large number of independent random variables x_k:

$$S = \sum_k^N x_k . \tag{1}$$

The x_k's are samples chosen at random from N distributions, not necessarily the same, and we inquire, what is the distribution of their sum? The Central Limit Theorem of statistical theory, subject to rather wide restrictions, states that the sum will be distributed in an asymptotically Gaussian manner with a mean "m" and variance "σ_x^2" which are the sum of the individual N distributions; that is,

$$m = \sum^N m_k \tag{2}$$

$$\sigma_x^2 = \sum^N \sigma_k^2 \tag{3}$$

and the distribution of "S" is (m, σ), or

$$W(S) = \frac{1}{\sqrt{2\pi}} \frac{1}{\sigma_x} e^{-(s-m)^2/2\sigma_x^2} . \tag{4}$$

This result can be applied to our problem of antenna errors, since a given error is caused by random, and generally independent, contributions from a number of sources.

---

[2] Brown, J., "The Effect of a Periodic Variation in the Field Intensity Across a Radiating Aperture," J. Inst. Elec. Engrs. (London), 97, Part III:419 (1950)

[3] Cramer, H., "Mathematical Methods of Statistics," Princeton University Press (1946)

It will therefore be distributed in an approximately Gaussian manner whose mean the designer selects as the design value.

The result also indicates that the sum of a large number of dc or in-phase voltages or vectors will also be Gaussian. Furthermore, it can be shown that when a constant value "a" is added to our sum the Gaussian distribution is displaced by "a" and now is characterized by $(m + a, \sigma_x)$.

Next we consider the distribution of the magnitude

$$r = \left[\left(\sum^{N} x_k \right)^2 + \left(\sum^{N} y_k \right)^2 \right]^{\frac{1}{2}} \tag{5}$$

The individual sums are distributed, from Equation (5), in a Gaussian manner. The distribution of "r" is formed by two perpendicular normal distributions. If the individual distributions are equal and characterized by $(0, \sigma_x)$ then "r" is Rayleigh distributed; that is,

$$W(r) = \frac{r}{\sigma_x^2} \quad e^{-r^2/2\sigma_x^2} \tag{6}$$

as

$$r_k^2 = x_k^2 + y_k^2 \ ;$$

then

$$r^2 = x^2 + y^2 = \sigma_x^2 + \sigma_y^2 = 2\sigma_x^2 = 2\sigma_y^2.$$

We can write this quantity simply as σ and write the Rayleigh distribution in the usual notation

$$W(r) = \frac{2r}{\sigma^2} \quad e^{-r^2/\sigma^2}. \tag{7}$$

We see that the Rayleigh distribution is characterized by a single quantity, the mean square of r_k. This distribution occurs in a number of physical problems. One of these is the two-dimensional random walk. If a particle suffers a large number of random displacements (with all directions equally likely) then its final position is given by Equation (5) and its probability distribution by Equation (7) with σ^2 equal to the mean square of its displacements r_k. Furthermore, the resultant sum of a large number of random voltages of arbitrary phase also satisfied the Rayleigh distribution,[4] since this resultant voltage is merely the root means square of the sum of the component voltage sums as given by Equation (5).

Blake[5] has shown that when a constant displacement "a" is added to the Rayleigh distribution or if we consider the distribution of r, where

$$r = \left[\left(a + \sum x_k \right)^2 + \left(\sum y_k \right)^2 \right]^{\frac{1}{2}}, \tag{8}$$

---

[4] Lord Rayleigh, "Theory of Sound," New York: Dover (1945), pp. 35-42

[5] Blake, L. V., "Reflections of Radio Waves from a Rough Sea," Proc. Inst. Radio Engrs., 38:301-304 (March 1950)

the result is distributed in a modified Rayleigh manner given by

$$W(r) = \frac{2r}{\sigma^2} e^{-(a^2 + r^2)/\sigma^2} I_0\left[\frac{2ar}{\sigma^2}\right], \tag{9}$$

where I_0 is the modified Bessel Function.

Figure 1 shows this modified Rayleigh distribution for various values of the displacement "a." For small values of "a" this distribution approaches the Rayleigh curve; and for large values of "a," due to the asymptotic behavior of the Bessel Function, we obtain

$$W(r) \longrightarrow \frac{1}{\sqrt{\pi}} \frac{1}{\sigma} \sqrt{\frac{r}{a}} e^{-(a - r)^2/\sigma^2} \tag{10}$$

or approximately Gaussian behavior.

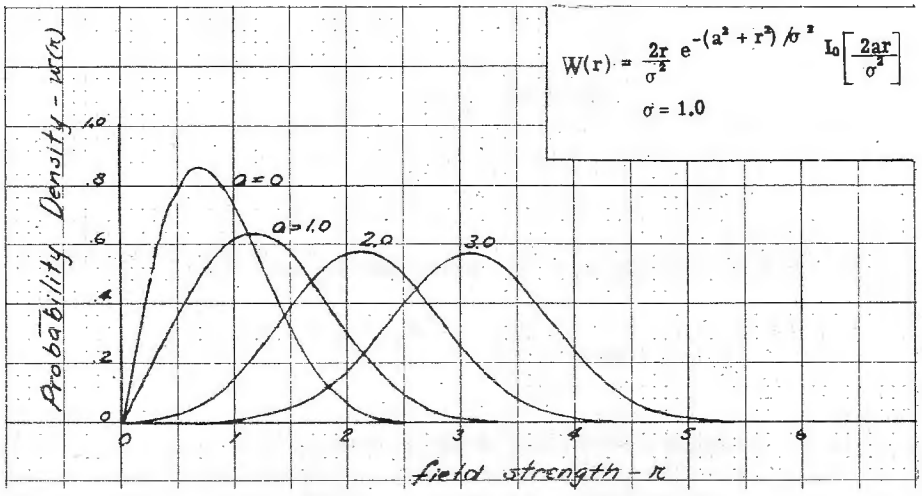

Figure 1 - Rayleigh and modified Rayleigh distribution

Another quantity of interest is the cumulative probability; that is, the probability of a sum being below some value, say r_0. This is given in terms of distribution function by

$$P\left[0 < r < r_0\right] = \int_0^{r_0} W(r)\, dr. \tag{11}$$

Figure 2 shows the cumulative probability for the distributions plotted in Figure 1.

APPLICATION TO AN ARRAY OF DISCRETE ELEMENTS [6]

Since the modified Rayleigh distribution can be applied to the sum of voltages of random phase, we can apply it to a number of electrical problems. These include the

6 Presented at the National Convention, I.R.E., March 1951, under "Physical Realizability of Low Side Lobes in Broadside Arrays"

distribution or likelihood of a given (a) voltage standing wave ratio on a transmission line caused by randomly located discontinuities, (b) the radar return from a group of random scatterers, (c) transmission in the rejection band of an electrical filter caused by errors in its circuit components, and (d) side-lobe level of an antenna caused by aperture excitation errors.

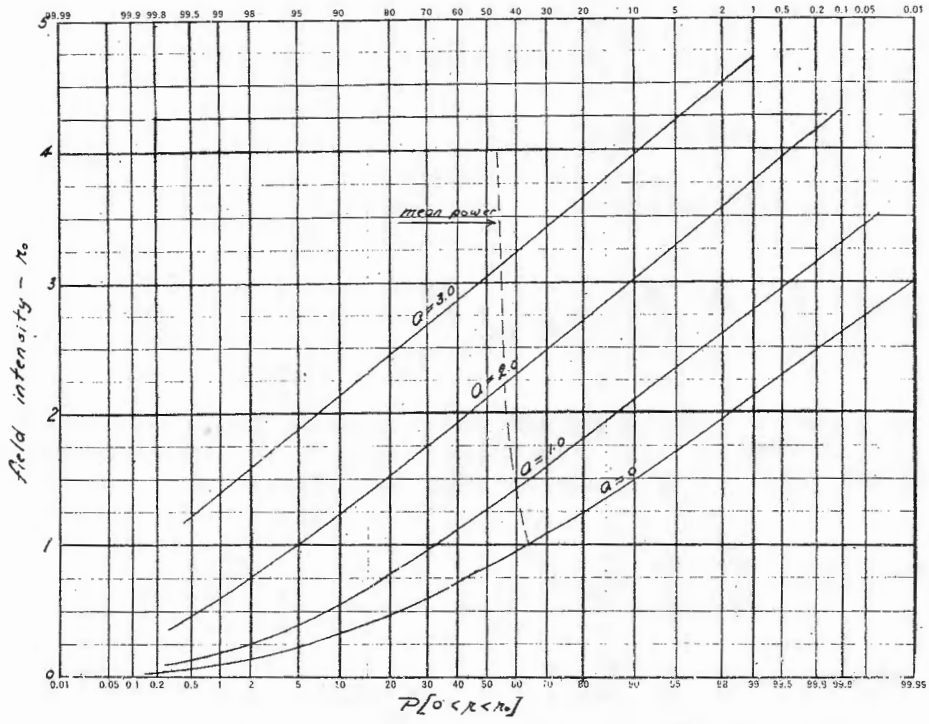

Figure 2 - Modified Rayleigh cumulative probability ($\sigma = 1.0$)

In the last-mentioned problem let us consider an array of MN elements spaced a distance "d" apart, and a quarter wave in front of a reflecting screen. Exclusive of distance and proportionality factors, the far-field field-component intensities are given by[7]

$$E_\theta(\theta,\phi) = \cos\theta\cos\phi \sum_n^N \sum_m^M I_{nm}\, e^{jk\sin\theta\left[md\cos\phi + nd\sin\phi\right]} \tag{12}$$

$$E_\phi(\theta,\phi) = \sin\phi \sum_n^N \sum_m^M I_{nm}\, e^{jk\sin\theta\left[md\cos\phi + nd\sin\phi\right]} \tag{13}$$

The coordinates are the usual right-handed system, with the array in the xy plane and directed along the z or θ=0 axis. The current is assumed to flow in the x-direction. The above formulas should be multiplied by a screen factor of $\sin(\pi/2\cos\theta)$; we shall, however, use the closely related function $\sqrt{\cos\theta}$ to preclude latter integration difficulties.

Now let us consider the individual element currents independently in error, both in phase and magnitude; that is, our currents become $I_{mn}(1 + \Delta_{mn})e^{j\delta}{}_{mn}$. The power patterns may be obtained from Equations (12) and (13) by forming the complex conjugate.

[7] Silver, S., "Microwave Antenna Theory and Design," New York: McGraw-Hill (1949), p. 89

Writing the summation term only, we have

$$P(\theta,\phi) \alpha \sum_{m}^{M} \sum_{n}^{N} \sum_{p}^{M} \sum_{q}^{N} I_{mn} I^{*}_{pq} \left(1 + \Delta_{mn}\right)\left(1 + \Delta_{pq}\right) \times$$

$$e^{jk \sin\theta \left[(m-p)\, d \cos\phi + (n-q)\, d \sin\phi \right]} \times$$

$$e^{j\left(\delta_{mn} - \delta_{pq}\right)}. \tag{14}$$

The desired or no-error pattern is

$$P_{0}(\theta,\phi) \alpha \sum_{m}^{M} \sum_{n}^{N} \sum_{p}^{M} \sum_{q}^{N} I_{mn} I^{*}_{pq}\, e^{jk \sin\theta \left[(m-p)\, d \cos\phi + (n = q\, d \sin\phi \right]}. \tag{15}$$

Let us now compute the "system average" pattern, that is, the average pattern of a large number of similar arrays. Designating this pattern by $\overline{P(\theta,\phi)}$ and assuming, as is likely, that the mean error is zero or that $\overline{\Delta_{mn}} = \overline{\delta_{mn}} = 0$, we have

$$\overline{P(\theta,\phi)} = \overline{\Delta^2} \sum_{m}^{M} \sum_{n}^{N} I^{2}_{mn} +$$

$$\sum_{m}^{M} \sum_{n}^{N} \sum_{p}^{M} \sum_{q}^{N} I_{mn} I^{*}_{pq} \left[\overline{\cos y} + \overline{j \sin y} \right] \times$$

$$e^{jk \sin\theta \left[(m-p)\, d \cos\phi + (n-q)\, d \sin\phi \right]} \tag{16}$$

where we have let $y = \delta_{mn} - \delta_{pq}$ and realized that the mean of the sum of independent variables is the sum of the means.

We must now evaluate the mean of cos y and sin y, where our fundamental random variable is "δ." We may assume that "δ" is distributed in a normal manner. This will be asymptotically true if the phase error is due to a number of causes and such errors are small. Then "y" becomes a random variable generated as the difference of two samples chosen from a normal distribution. The distribution of y, commonly called the "range," is given by

$$W(y) = \int_{-\infty}^{\infty} W_{,}(\delta)\, W(\delta + y)\, d\delta \tag{17}$$

where

$$W_{,}(\delta) = \frac{1}{\sqrt{2\pi\overline{\delta^2}}}\, e^{-\delta^2 / 2\overline{\delta^2}} \tag{18}$$

Performing the integration we obtain

$$W(y) = \frac{1}{\sqrt{4\pi\overline{\delta^2}}}\, e^{-y^2 / 4\overline{\delta^2}} \tag{19}$$

and

$$\overline{\cos y} = \int_{-\infty}^{\infty} \cos y\, W(y)\, dy = e^{-\overline{y^2}/2} = e^{-\overline{\delta^2}} \tag{20}$$

$$\sin y = \int_{-\infty}^{\infty} \sin y\, W(y)\, dy = 0. \tag{21}$$

Applying these results to Equation (16), making use of Equation (15), and adding the two component powers, Equation (12) and (13),

$$\overline{P(\theta,\phi)} = P_0(\theta,\phi)\, e^{-\overline{\delta^2}} + s(\theta,\phi)\left[\overline{\Delta^2} + 1 - e^{-\overline{\delta^2}}\right] \sum_m^M \sum_n^N I_{mn}^2 \tag{22}$$

where

$$s(\theta,\phi) = \cos\theta \left[\cos^2\theta \cos^2\phi + \sin^2\phi\right].$$

Normalizing our pattern and calling $\overline{\epsilon^2}$ the total mean square error,

$$\overline{\epsilon^2} = \left[\overline{\Delta^2} + \left(1 - e^{-\overline{\delta^2}}\right)\right] e^{\overline{\delta^2}} \approx \overline{\Delta^2} + \overline{\delta^2} \tag{23}$$

$$\overline{p(\theta,\phi)} = p_0(\theta,\phi) + s(\theta,\phi)\, \overline{\epsilon^2} \frac{\sum^M \sum^N I_{mn}^2}{\left(\sum^M \sum^N I_{mn}\right)^2}. \tag{24}$$

Equation (24) gives the "average system" pattern. We see that the effect of the error distribution is to add an essentially constant power level proportional to the mean squared error. Individual arrays and particular spatial directions will show side-lobe radiation differing from this constant value. However, such radiation will be distributed in a Guassian manner about the undistorted pattern when the error contribution is comparatively small, and in a Rayleigh manner for large errors when the original side-lobe radiation may be neglected. The formula also indicates that relatively smaller spurious radiation will occur for a larger number of elements; in fact, the error contribution depends approximately on 1/NM. Hence, for a given current precision, low side lobes are more readily realized with large antennas.

Figure 3 shows these results graphically for the special case of a 25-element array (M = 25, N = 1) designed with a Tschebyscheff distribution to yield side lobes of 29 db. Figure 4 shows both the no-error pattern and a pattern obtained by adding to each element a 40-percent current at a random phase ($\overline{\epsilon^2} = 0.16$). Finally, Figure 5 shows a plot of the distribution of side-lobe magnitudes as obtained from the computed error curve in Figure 4 and compares it to the theoretical Rayleigh distribution. Our mathematics is thus checked.

Let us now consider the effect of the current errors on the antenna gain. The gain G_0 of the theoretical antenna is given by

$$G_0 = \frac{4\pi}{\int p_0(\theta,\phi)\, d\Omega}. \tag{25}$$

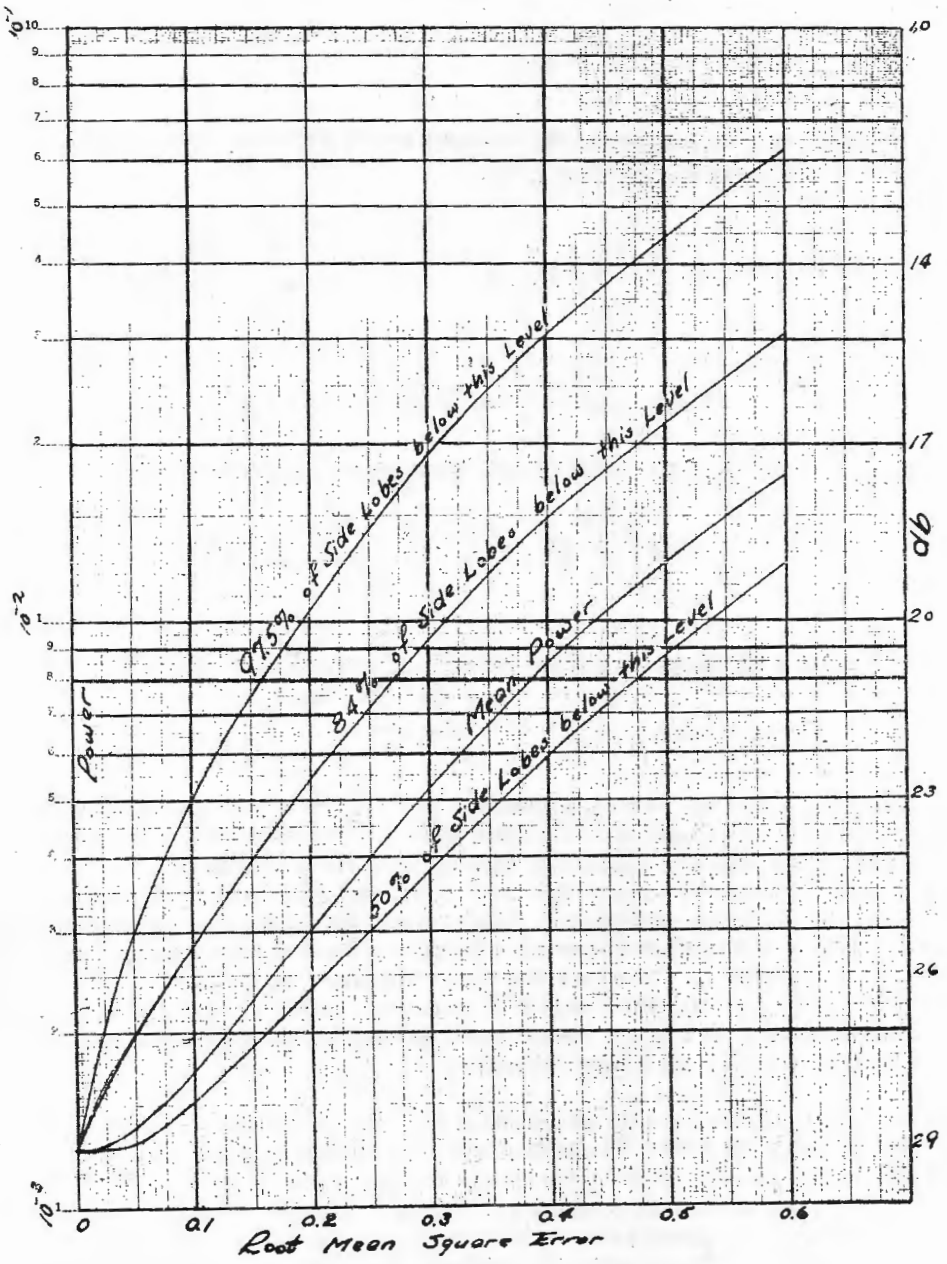

Figure 3 - Side-lobe distribution of 25-element broadside array designed for 28-db side lobes, Tschebyscheff distribution, computed at maximum of design lobes

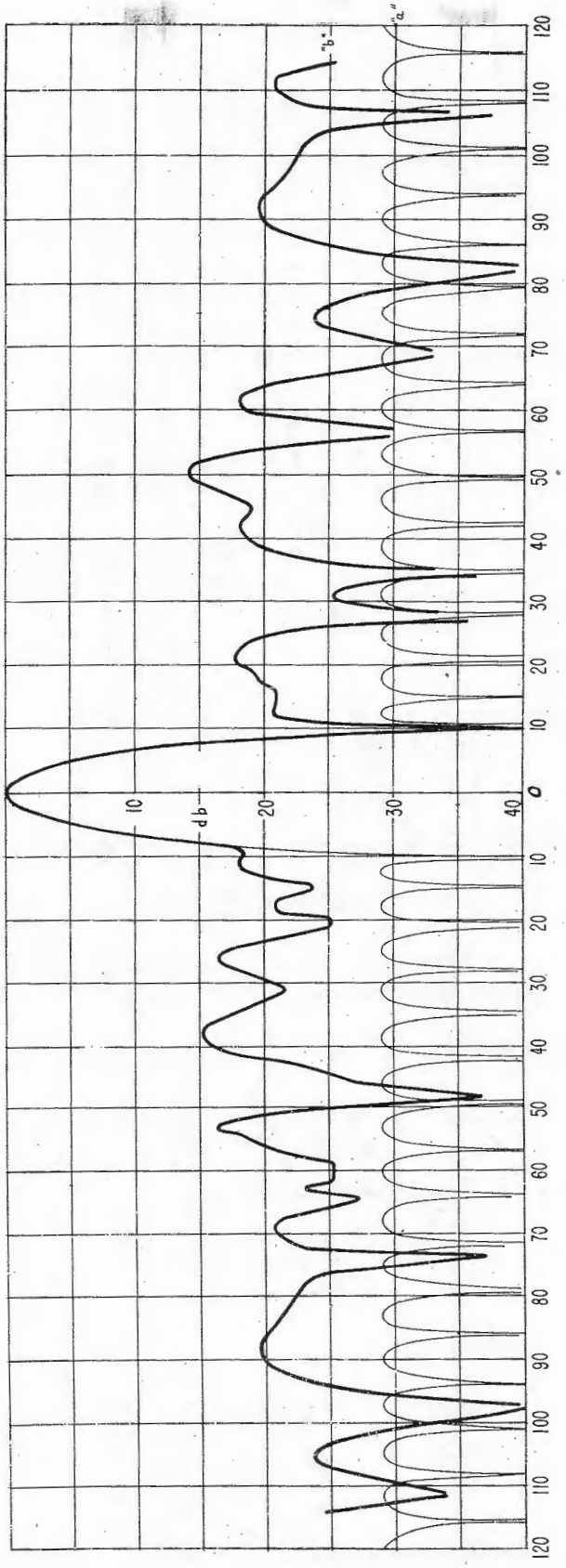

Figure 4 - Theoretical antenna patterns, "a" with taper to yield 29-db side lobes, "b" with "a" but with 40-percent random currents

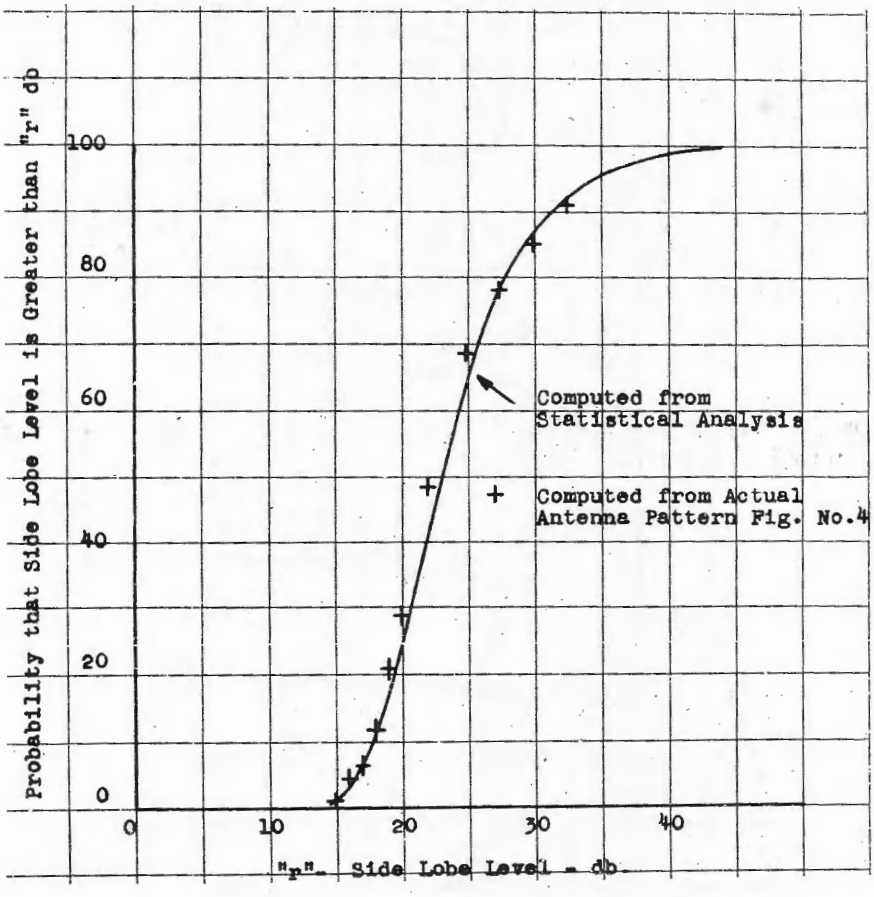

Figure 5 - Distribution of side-lobe magnitudes obtained from the computed-error curve of Figure 4

Letting G be the gain of the antenna with the error distribution, we have, upon performing the evident integrations,

$$\frac{G}{G_0} = \frac{1 + \overline{\epsilon^2} \dfrac{\sum\sum I_{mn}^2}{\left(\sum\sum I_{mn}\right)^2} e^{\overline{\delta^2}}}{1 + \frac{3}{16} G_0 \epsilon^2 \dfrac{\sum\sum I_{mn}^2}{\left(\sum\sum I_{mn}\right)^2} e^{\overline{\delta^2}}} . \tag{26}$$

As G_0 is usually a large number,

$$\frac{G}{G_0} \approx \frac{1}{1 + \frac{3}{16} G_0 \overline{\epsilon^2} \dfrac{\sum\sum I_{mn}^2}{\left(\sum\sum I_{mn}\right)^2} e^{\overline{\delta^2}}} . \tag{27}$$

Into Equation (27) we may insert the value for G_0, or using an approximate expression for the gain of a broadside array we have for most practical purposes:

$$\frac{G}{G_0} \quad \frac{1}{1 + \frac{3\pi}{16}\overline{\epsilon^2}} \tag{28}$$

APPLICATION TO A CONTINUOUS APERTURE [8]

In general, the same statistical considerations apply to the aperture antenna as to the discrete array. However, an additional factor is introduced which alters the final result. In the discrete case we assumed that the error current in one element was independent of the error currents in adjacent elements. This assumption is untenable in an aperture antenna because if the error is large at one point it will probably be large in the immediate neighborhood. The size of the correlated region will be found to affect both the magnitude and the directional characteristics of the spurious radiation.

For our discussion, let us consider a circular aperture excited by an electric current in the x-direction. Figure 6 shows the coordinate system. Since we are interested primarily in parabolic mirror, we will assume only a pure phase error.

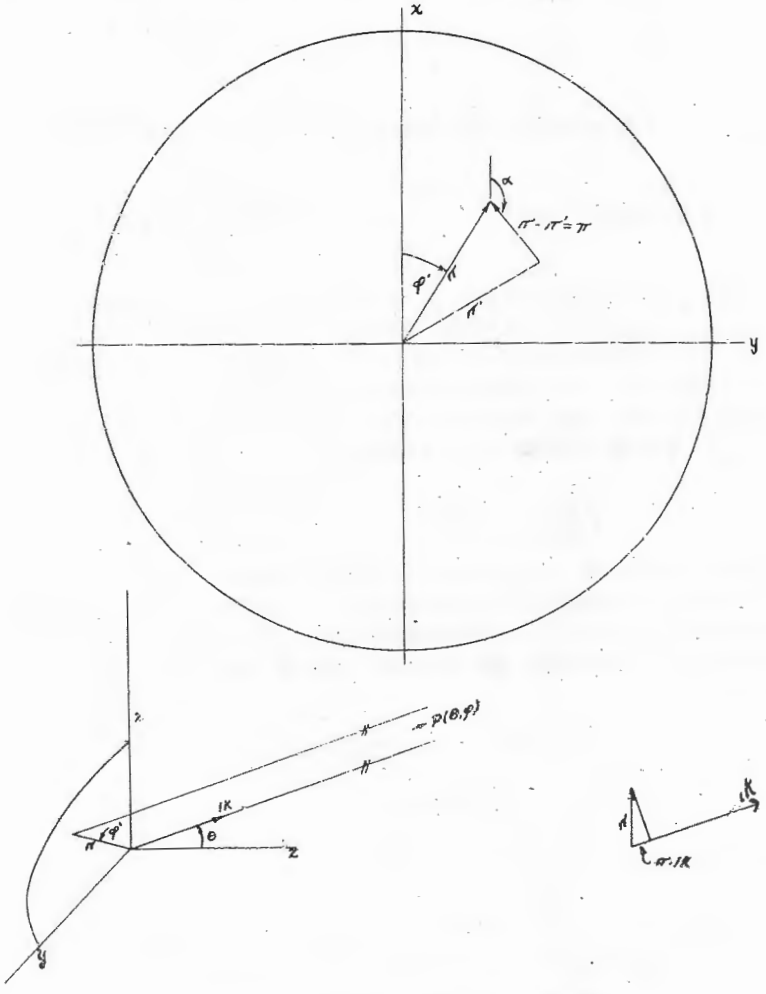

Figure 6 - Coordinate system

[8] To be presented at National Convention, I.R.E., 1952, under "Tolerances on Paraboloidal Mirror"

Following closely our discrete analysis and avoiding needless repetition, Equations (12) and (13) hold, provided we replace the summations with integrations over the aperture. For the paraboloid, the integration is performed over the undistorted mirror surface instead of over the plane aperture. This integral with a position-dependent phase error is

$$E(\theta,\phi) = \int J_x(\tau)\, e^{j\, k\cdot\tau}\, e^{j\delta(\tau)}\, dS \tag{29}$$

and the power pattern (corresponding to Equation (14) becomes

$$P(\theta,\phi) = \iint J_x(\tau)\, J^*(\tau')\, e^{jk\cdot(\tau-\tau')}\, e^{j\left[\delta(\tau)-\delta(\tau')\right]}\, dS_\tau\, dS_{\tau'} \tag{30}$$

changing the vector position variable, so that $(\tau - \tau') = \pi$.

$$P(\theta,\phi) = \iint J(\pi+\tau')\, J^*(\tau')\, e^{jk\cdot\pi}\, e^{j\delta(\pi+\tau')-\delta(\tau')}\, dS_\tau\, dS_{\tau'}. \tag{31}$$

With the same notation as previously used we obtain for the mean pattern

$$\overline{P(\theta,\phi)} = \iint J(\tau+\pi)\, J^*(\tau)\, e^{j\,k\cdot\pi}\left[\overline{\cos y} + i\,\overline{\sin y}\right] dS_\tau\, dS_{\tau'}. \tag{32}$$

Now "y," the phase difference of two points on the aperture spaced a distance π apart, has zero mean since positive and negative errors are equally likely. For large values of τ the phase errors are uncorrelated, and the means square has the same value as previously. For $\tau = 0$ the mean square phase difference is obviously zero. The mean square value therefore depends on τ, and we have only its limiting values. We must assume some functional form to fit these conditions. Assuming that

$$\overline{y^2(\tau)} = \overline{2\delta^2}\left[1 - e^{-\tau^2/C^2}\right] \tag{33}$$

where "C" may be defined as a "correlation interval," that is, that distance "on average" where the errors become essentially independent. In using Equation (33) we are making the further assumption that the errors are uniformly distributed over the aperture. Inserting into Equation (32) with the aid of Equation (20) and defining the aperture autocorrelation function,

$$\phi(\pi) = \frac{\int J(\tau+\pi)\, J^*(\tau)\, dS_\tau}{\int J^2(\tau)\, dS_\tau} \tag{34}$$

we obtain

$$\overline{P(\theta,\phi)} = e^{-\overline{\delta^2}} \int J^2(\tau)\, dS_\tau \int \phi(\pi)\, e^{j\,k\cdot\pi}\, e^{\overline{\delta^2}\, e^{-\tau^2/C^2}}\, dS_\tau. \tag{35}$$

Expanding the exponential and realizing that the undistorted pattern is

$$P_0(\theta,\phi) = \int J^2(\tau)\, dS_\tau \int \phi(\pi)\, e^{j\,k\cdot\pi}\, dS_\tau \tag{36}$$

we have

$$\overline{P(\theta,\phi)} = P_0(\theta,\phi)\, e^{-\overline{\delta^2}} + e^{-\overline{\delta^2}} \int J^2(\tau)\, dS_\tau \sum_{n=1}^{\infty} \int \phi(\pi) e^{j k\cdot\tau} \frac{\left[\overline{\delta^2}\right]^n}{n!} e^{-\frac{n\tau^2}{c^2}} \tau\, d\tau\, d\alpha . \quad (37)$$

Now $\phi(\pi)$ is a slowly varying function with $\phi(0) = 1$, whereas the exponential essentially vanishes for $\tau > C$. Realizing that

$$k \cdot \pi = \frac{2\pi\tau}{\lambda} \sin\theta \cos(\phi - \alpha),$$

the "α" integration may be performed and, with $u = \sin\theta$,

$$\overline{P(\theta,\phi)} = P_0(\theta,\phi)\, e^{-\overline{\delta^2}} + e^{-\overline{\delta^2}} \int J^2(\tau)\, dS_\tau \sum_{n=1}^{\infty} \frac{\left[\overline{\delta^2}\right]^n}{n!} 2\pi \int_0^{\infty} J_0\left(\frac{2\pi u \tau}{\lambda}\right) e^{-\frac{n\tau^2}{c^2}} \tau\, d\tau . \quad (38)$$

The last integration may be performed by the method of residues

$$\overline{P(\theta,\phi)} = P_0(\theta,\phi)\, e^{-\overline{\delta^2}} + \overline{\delta^2}\, \frac{c^2\pi}{1}\, e^{-\overline{\delta^2}} \left[\sum_{1}^{\infty} \frac{\left[\overline{\delta^2}\right]^{2(n-1)}}{n!n}\, e^{-\pi^2 u^2 c^2/n\lambda^2}\right] \int J^2(\tau)\, dS. \quad (39)$$

Normalizing by dividing by the factor $\left[\int J(\tau)\, dS\right]^2$ and defining the normal gain G_0,

$$G_0 = \frac{4\pi}{\lambda^2} \frac{\left[\int J(\tau)\, dS\right]^2}{\int J^2(\tau)\, ds},$$

we obtain

$$\overline{p(\theta,\phi)} = p_0(\theta,\phi) + \frac{4c^2\pi^2\overline{\delta^2}}{\lambda^2 G_0}\, s(\theta,\phi) \left[\sum_{n=1}^{\infty} \frac{\left[\overline{\delta^2}\right]^{n-1}}{n!n}\, e^{-\pi^2 u^2 c^2/n\lambda^2}\right], \quad (40)$$

where we have further summed the two component powers and introduced our obliquity and screen factor.

Equation (40) is comparable to Equation (24) and gives the average system pattern. For small phase errors we need to consider only the first term of the series; the disturbing pattern then is

$$\frac{4c^2\pi^2\overline{\delta^2}}{\lambda^2 G_0}\, e^{-\pi^2 u^2 c^2/\lambda^2} . \quad (41)$$

We note that the spurious radiation is again proportional to the mean-squared error; in addition it is proportional to the square of the correlation interval in wavelengths. Furthermore, this radiation is no longer essentially uniformly spatially distributed but becomes directionally directed along the axis of the aperture. The directivity increases

with the size of the correlation region; so that for "rough" reflectors, where the correlation interval is small, energy is scattered essentially uniformly. This is not at all surprising physically, for regions large compared to a wavelength (which are at the same phase) will scatter more strongly and more directively.

The higher-order terms of Equation (40) are of lower directivity and hence have the same effect as a smaller correlation interval. This again has physical basis due to the periodic nature of the trigonometric functions.

The above analysis indicates the importance of the correlation region on the scattered energy. If errors are unavoidable in a reflecting surface (rivet heads, etc.), they should be small in extent—small compared to a wavelength—and they should have a negligible effect on the mirror performance.

The reduction in gain can be obtained as in the discrete case. Only the results for small phase errors and the extreme cases are given here:

Small correlation interval:
$$\frac{G}{G_0} \simeq \frac{1}{1 + \frac{\pi \overline{\delta^2}}{4} \frac{c^2 \pi^2}{\lambda^2}} \tag{42}$$

Large correlation interval:
$$\frac{G}{G_0} = e^{-\overline{\delta^2}} \simeq 1 - \overline{\delta^2} \tag{43}$$

It is interesting to compare the last result with that obtained by Spencer [9], by a much simpler analysis—namely, that the fractional loss of gain is equal to mean-square phase error weighted according to the excitation amplitude. With the simplifications made, this checks the above result.

Finally, Figure 7 shows the side-lobe radiation to be expected from typical parabolas. Figure 8 shows the polar diagram and Figure 9 the reduction in gain. It should be noted that if the phase errors are normally distributed, then Equation (40) is not restricted to small phase errors.

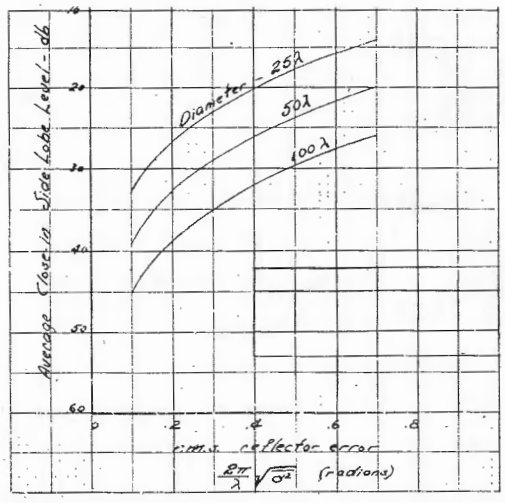

Figure 7 - Spurious radiation of paraboloid, parabolic mirror, cosine squared illumination, correlation interval $c = \lambda$

[9] Spencer, Roy C., "A Least Square Analysis of the Effect of Phase Errors on Antenna Gain," Report No. E5025, AFCRC, January 1949

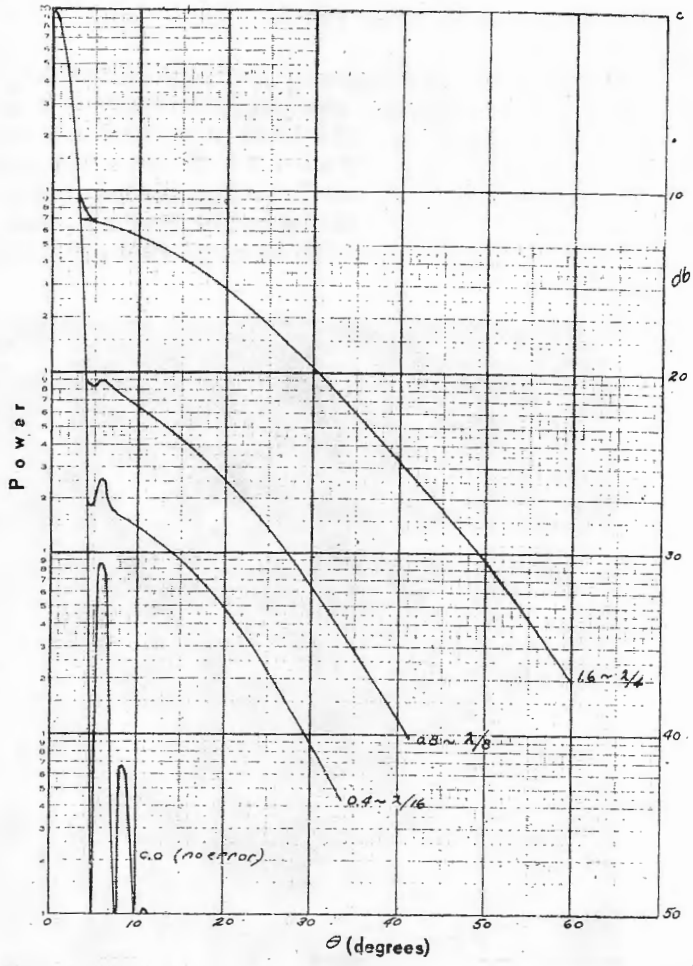

Figure 8 - Average system pattern, 30-inch aperture, X-band, correlation interval = 2, D = 24λ, rms phase error in radians, E-plane

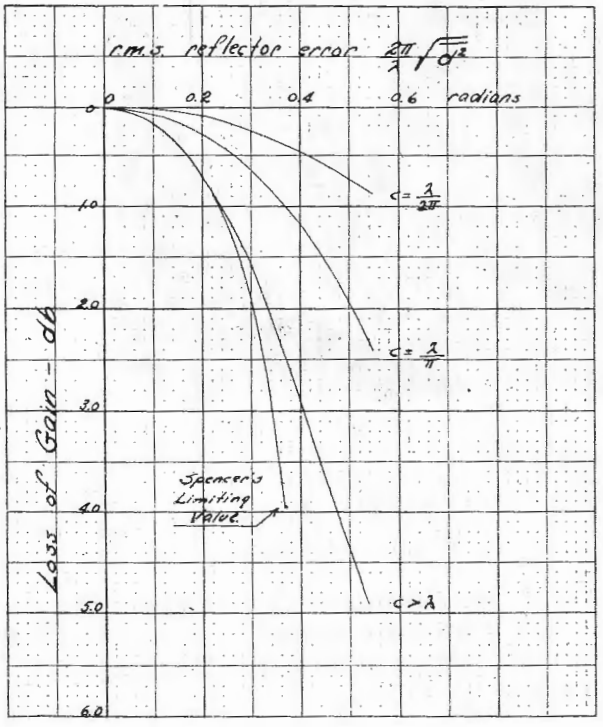

Figure 9 - Reduction of gain of parabolic mirror

EXPERIMENTAL CONFIRMATION

To provide some experimental confirmation for this theory, a 30-inch parabolic dish w distorted in a prescribed and approximately random fashion. Indentations of the surface were made by a shaped die. The depth of indentations were chosen at random from a Gauss population with a variance to yield a 2.5-db reduction in gain. This caused reflector phase errors in some portions of the surface that exceeded a half wavelength when the dish was operate at X-band. Figure 10 shows a photograph of this dish. Gain comparison measurements with an undistorted parabola indicated the expected gain reduction within experimental error.

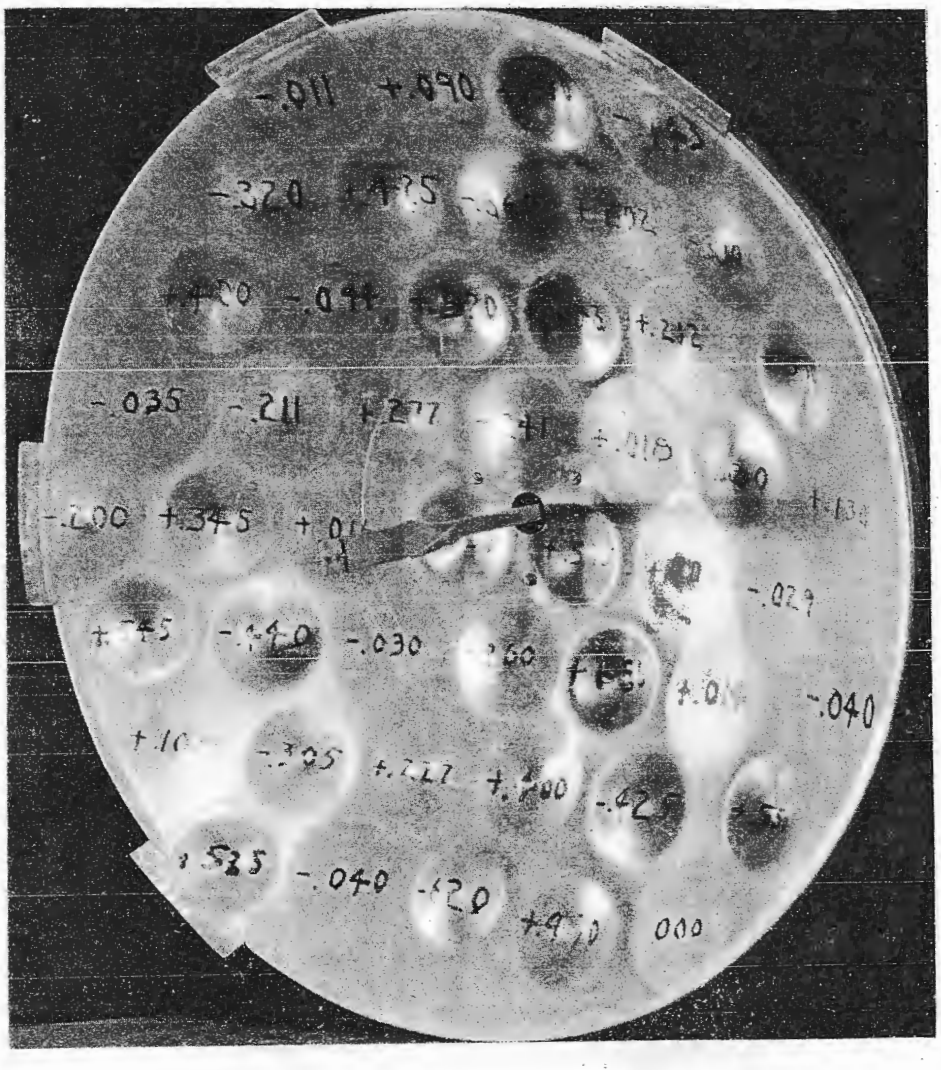

Figure 10 - Distorted 30-inch parabolic dish used in the experimental confirmation of the theory

SUMMARY

Formulas are derived for the loss of gain and the average spurious radiation due to aperture excitation errors for both the discrete array and the continuous aperture. These

results may be applied to a particular type of antenna. This has been done for the slot array by Bailin and Ehrlich [10] who used a similar theory.

ACKNOWLEDGMENT

The assistance and guidance of Prof. L. J. Chu of M.I.T. has, to a large extent, made this work possible.

[10] Bailin, L. L., and Ehrlich, M. J., "Factors Affecting the Performance of Linear Arrays," Hughes Aircraft Co. report

* * *

Antenna Pattern Calculation for Asymmetrical Aperture Distributions

Charles C. Allen
General Electric Company
Schenectady, New York

Abstract of Presentation at NRL Side-Lobe Conference, April 23, 1952

INTRODUCTION

The method of calculation presented in this paper is a direct approach to obtaining the far-field pattern of an antenna from its aperture distribution. Instead of approximating the aperture distribution in some manner to obtain an integrable function, the actual amplitude and phase distribution is used in performing a numerical integration on automatic punch-card machines. The approximation is in the integral rather than the integrand and can be made as close as desired by selecting a sufficient number of increments across the aperture. The method is perfectly general and can be applied to a double integral having an integrand which represents a nonseparable aperture distribution.

The examples presented are for separable distributions in a rectangular aperture for which the applicable equations in normalized form are:

Aperture Distribution: $$F(x) = f(x)\, e^{j\psi(x)} \tag{1}$$

Pattern: $$E(u) = a\int_{-1}^{1} f(x)\, e^{j\Phi(x)}\, dx \tag{2}$$

$$\Phi(x) = ux + \psi(x) \tag{3}$$

$$u = \beta a \sin\theta \tag{4}$$

where $2a$ = aperture length, $\beta = 2\pi/$ wavelength, and θ = angle in actual units. For evaluation on automatic punch card machines, Equation (2) becomes:

$$E(u) \doteq a\sum_{i=1}^{n} f(x_i)\, \cos\Phi(x_i)\, \Delta x + j\, a\sum_{i=1}^{n} f(x_i)\, \sin\Phi(x_i)\, \Delta x \doteq g(u)\, e^{j\alpha(u)} \tag{5}$$

The aperture gain factor relative to that for uniform illumination of the aperture requires evaluation of the integral

$$P = a\int_{-1}^{1}\left[f(x)\right]^2 dx = a\sum_{i=1}^{n}\left[f(x_i)\right]^2 \Delta x \tag{6}$$

The magnitude patterns, $g(u)$, and phase patterns, $\alpha(u)$, were evaluated by this method for the cases of (1) asymmetrical amplitude with linear phase, (2) symmetrical amplitude with nonlinear phase, and (3) combined asymmetrical amplitude and nonlinear phase.

ASYMMETRICAL AMPLITUDE AND LINEAR PHASE DISTRIBUTION

The patterns for this case have conjugate symmetry about the direction of maximum intensity; that is, the magnitude patterns have even symmetry, and the phase patterns have

odd symmetry. The phase pattern, $\alpha(u)$, permits determination of the aperture phase center.

For examples of this case, an asymmetrical parabolic reflector extending from near the vertex to the latus rectum is used to obtain an asymmetrical amplitude distribution. The feed is placed at the focus to obtain a uniform phase distribution.[1] The feed pattern is taken as $\cos^r \Omega$ with Ω measured from the feed axis. Such a pattern agrees well with experimental patterns for the angles subtended by the reflector. The exponent r is chosen in conjuction with the angle Ω_0 between the feed and reflector axes to taper the intensity at the edges of the aperture to 6, 10, 14, and 20 decibels down from the maximum intensity.

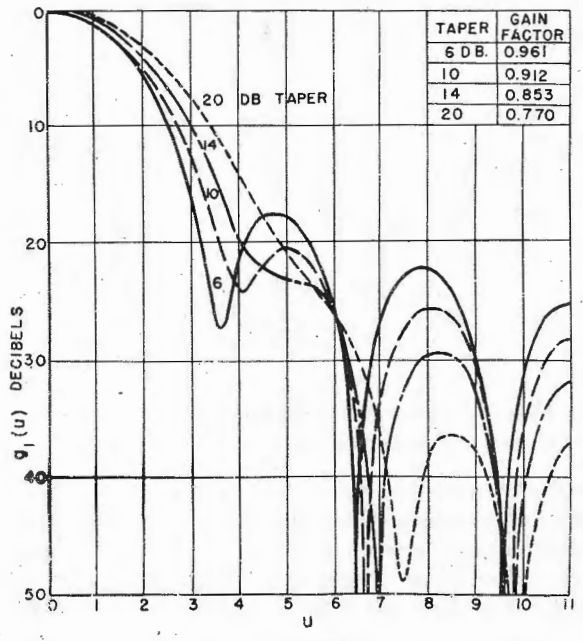

Figure 1 - Patterns with linear phase distributions and various asymmetrical illumination tapers

The magnitude patterns, g(u), for this case are given in Figure 1. It is seen that the first null is filled in to a greater extent for greater illumination taper. This is caused by the sine term in Equation (5) which for a symmetrical amplitude distribution with uniform phase would be zero for all values of u.

II. SYMMETRICAL AMPLITUDE AND PHASE DISTRIBUTION

The examples for this case extend the study of quadratic and cubic phase distributions by other workers [1,2] to combinations of quadratic and cubic phase distribution together with amplitude distributions of intermediate taper. The amplitude distribution is taken as

$$f(x) = M + N \cos \frac{\pi}{2} x$$

with M and N chosen to give illumination tapers of 0, 10, and infinite decibels. Ten phase distributions of the form

$$\psi(x) = -\delta(Ax^2 + Bx^3)$$

are used with each of the three amplitude distributions to obtain ten sets of patterns. Five pairs of values of A and B are used (1,0), (1,0.5), (1,1), (0.5,1), and (0,1) together with δ equal to $\pi/4$ and $\pi/2$.

A typical set of magnitude patterns is given in Figure 2. The effects of both quadratic phase distribution, which fills in the nulls, and cubic phase distribution, which tilts the pattern and makes it asymmetrical, are seen here. In practice, a cubic phase distribution is generally accompanied by a linear phase distribution of opposite sign which tilts the entire pattern so as to make the coma lobe and the main beam appear on opposite sides of the point u equals zero.

---

1. Spencer, R. C., and Austin, P. M., "Tables and Methods of Calculation for Line Sources," RL Report 762-2, March 30, 1946

2. Friss, H. T., and Lewis, W. D., "Radar Antennas," Bell Sys. Tech. Jour., 26: 219-247, April 1947

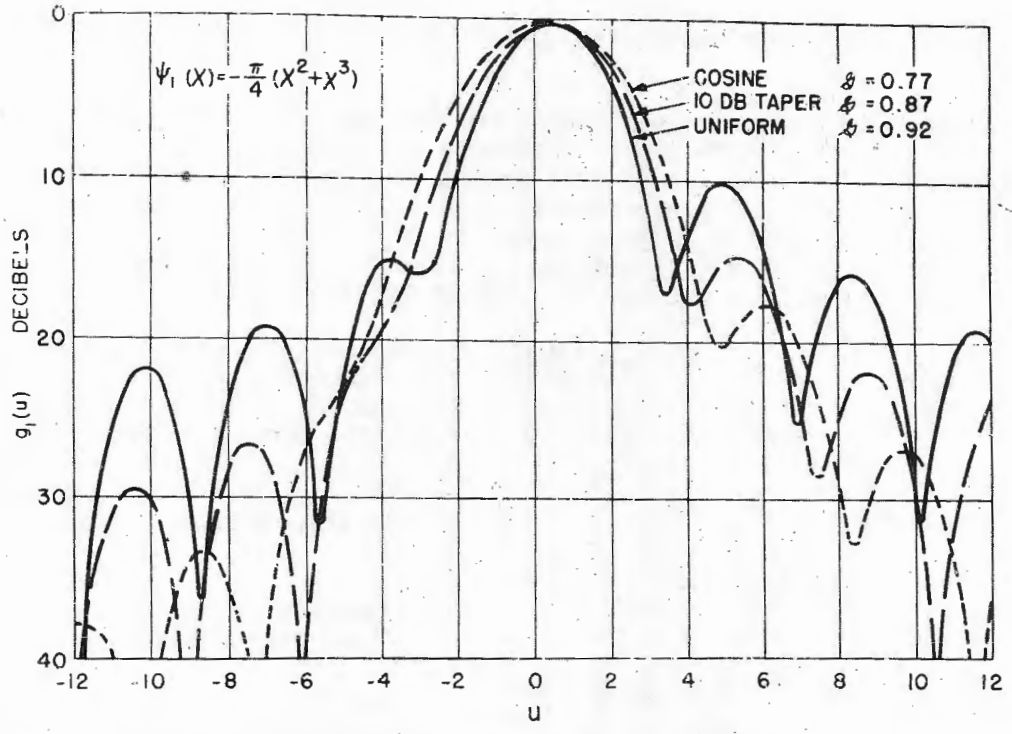

Figure 2 - Typical magnitude patterns for nonlinear phase distribution and symmetrical illumination tapers

The complete set of patterns can be used to synthesize the pattern expected for a given distribtuion. This is helpful in obtaining semiquantitative information regarding expected side-lobe levels, beam tilt, beam broadening, and gain factor prior to evaluating the actual pattern. An example of such synthesis is given in the next case. This use of the set of patterns is considered more reliable than the use of some arbitrary criteria such as those given by Ruze.[3]

III. COMBINATION ASYMMETRICAL AMPLITUDE AND NONLINEAR PHASE DISTRIBUTIC

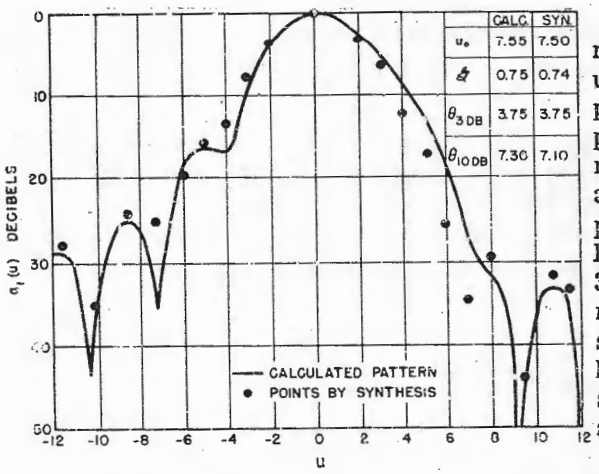

Figure 3 - Patterns for nonlinear phase and asymmetrical amplitude distribution (displacement of 0.06 focal length, $\frac{\ell}{\lambda} = 29$)

For examples of this case, the asymmetrical parabolic reflector of Case I is used with the feed displaced from the focus perpendicualr to the feed axis. The feed pattern is $\cos^5\Omega$, which tapers the illumination approximately 14 db to the edges of th aperture. The magnitude pattern for a displacement of 0.06 focal length, with the focal length equal to 29 wavelengths, is given in Figu 3. This is plotted relative to the direction of maximum intensity, u_0', given in the table. It is seen that the beam is tilted appreciably, a high coma lobe exists, and the first null and side lobe in the +u direction are completely absorbed into the main beam.

The black dots in Figure 3 were determined by using the set of patterns discusse

3. Ruze, J., "Wide-Angle Metal-Plate Optics," Proc. IRE, 38: 57, January 1950

under Case II to synthesize the pattern from its aperture distribution. The beam tilt, change in gain factor, change in beamwidth, and change in side-lobe level caused by the nonlinear phase distribution were determined for a 14-db tapered illumination by interpolation from the set of patterns. These changes were then applied to the 14-db taper pattern of Case I to obtain by synthesis the points in Figure 3.

Many scanning antennas and multiple-feed antennas involve aperture distributions of the type discussed in Case III. The distributions are generally warped asymmetrical surfaces in a three-dimensional plot. The method of calculation presented in this paper permits evaluation of the patterns for such antennas without recourse to functions approximating the aperture distribution. The method is also less tedious than those requiring extensive mathematical or graphical analysis.

* * *

The Effects of Mechanical Deviations in Radar Antenna Reflectors

John F. Dominy
Hazeltine Electronics Corporation

In the production of radar antenna reflectors a problem arises when the electrical performance must be held within a small percentage of that which is theoretically possible. Slight deviations from the desired reflector surface, which are inevitable in a produ tion run, will affect the electrical characteristics to some extent and may result in the reflector being rejected.

In the production testing of such reflectors, several alternative procedures are poss ble. One method is to conduct complete electrical tests on each unit; this is, of course, time consuming and expensive. Another method is to base the acceptance of the reflecto on a mechanical measurement of the surface, having first established an arbitrary limit for the allowable mechanical error. Since the area and distribution of the errors are fully as important as their magnitude, this method may require an extremely close mech ical tolerance, and a costly precision fabrication process, in order to make certain that the electrical characteristics will meet specifications. A third method consists of makin complete mechanical measurements of the surface, analyzing the results very carefully, and basing the acceptance or rejection, or the need for electrical tests, on the results of this analysis. Thus, the mechanical tolerances need not be as close with such a method. This paper will briefly describe such an analysis and its application in the testing of a hypothetical antenna reflector of an arbitrary type.

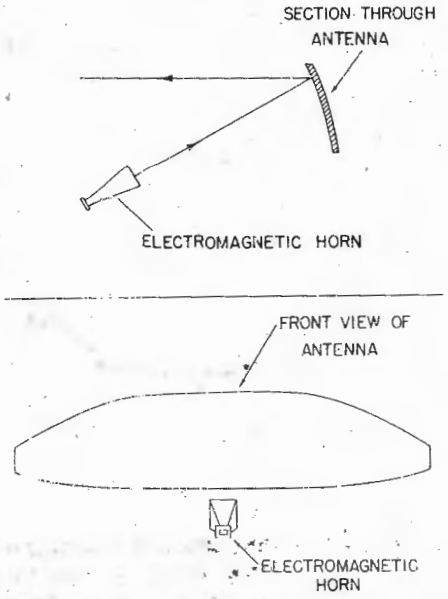

Figure 1 - Orange-peel paraboloid showing feed horn

The type of antenna selected is the "orange-peel paraboloid" as shown in Figure 1. A sectio is cut from the paraboloid in such a manner that the primary radiator which illuminates the anten will not obstruct the beam. The horn is designed so that the amplitude of illumination across the reflector surface will vary almost as the $\cos^2$ fu tion. For convenience, the distances along the lc dimension of the reflector have been expressed i degrees of the illumination function; the total len of the reflector is equal to 180 degrees. The illu nation becomes practically zero at the 90-degree points corresponding to the edges of the reflecto

The method of analysis is to divide the refle surface into a number of small areas, and to ass that the total radiation in any given direction is t vector sum of the individual radiations from eacl these small areas. It is further assumed that the ciple effect of small deviations from the true par surface is a change in the phase of the particular involved.

The procedure is to assume a direction in which it is desired to investigate the radiation, determine the amplitude and phase of each of the individual vectors, (each representing the radiation from one of the small areas), and plot these vectors graphically to determine the resultant. An analysis of this diagram will then show the effects of small deviations from the true surface on the amplitude of the resultant, and will thereby indicate the electrical performance to be expected.

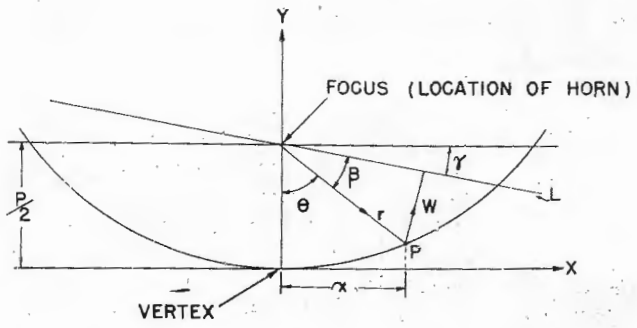

Figure 2 - Diagram for main lobe and side lobe calculations

The amplitude of each vector is proportional to the reflector area which it represents and to the illumination which this area receives. The phase of each vector can be determined by considering the geometry involved as shown in Figure 2. Referring to the diagram, we are interested in the radiation in a direction making an angle γ with the axis of the parabola. The phase relationship existing between the vectors making up the total radiation arriving at a distant target are the same as the phase relationships of the vectors considered along the line L, which is perpendicular to the direction of the target. To determine the phase of the radiation contributed by a small area at a distance x from the vertex, the total distance r + w must be determined and expressed in terms of wavelength. This can be done if the equation of the parabola and the angle γ are known. When all the distances (r + w) have been calculated for the various values of x, the value for x = 0 is subtracted from each, since we are interested only in the relative phase relationships between the vectors. Knowing the amplitude and phase of each vector, a vector diagram can be drawn to determine the resultant radiation in the desired direction.

In the vector diagram shown in Figure 3 the direction γ has been chosen to coincide approximately with the maximum of the side lobe on one side of the radiation pattern. The value of the resultant can be scaled from the diagram, and the power level of the side lobe can be determined by comparing the length of the resultant with the total length of all the vectors on the diagram.

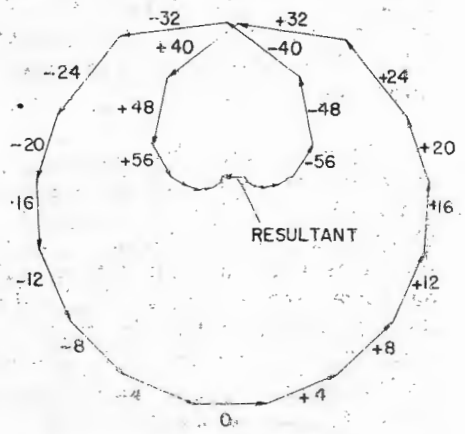

Figure 3 - Vector diagram for side lobes

The effect of a mechanical error in any given area of the reflector surface will be to change the phase angle of the vector corresponding to that area. It can be seen that a counterclockwise rotation of any of the vectors from +8 to +24 will have the effect of lengthening the resultant, while a clockwise rotation will shorten it. A similar statement can be made about the vectors from -8 to -24, except that opposite effects occur. Likewise, counterclockwise rotations of vectors from +40 to +56 or clockwise rotation of vectors from -40 to -56 will cause a shortening of the resultant. Similar results occur with the vectors from +72 to +88 and -72 to -88.

If we know how the errors are distributed over the surface of a given reflector, we can predict from the above vector diagram whether or not the side lobe will be strengthened.

The strengthening of one side lobe will be accompanied by the weakening of the other. W can show the error distribution, which causes large side lobes, as a function of distance along the reflector as in Figure 4. Positive errors in the black regions on the chart hav the same effect as negative errors in the shaded region, and vice versa. If positive erro occur in both a black region and a shaded region, the effects tend to cancel. Errors outs the black and shaded regions have very little effect on the magnitude of side lobes.

Other effects of errors in various regions of the chart are shown. These effects inc narrowing or widening of the main beam, strengthening of coma lobes, and the reduction of the maximum swing available when scanning.

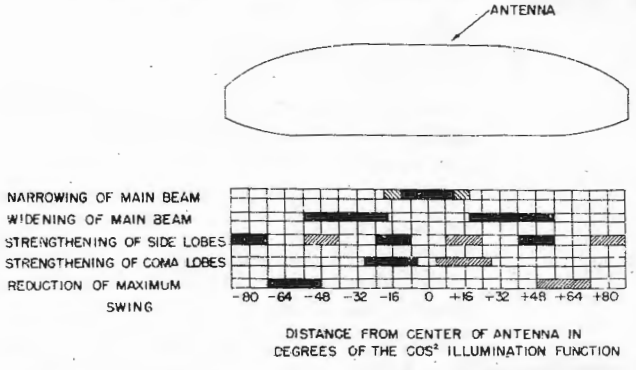

Figure 4 - Error distribution and the effect on electrical performance of antenna

Figure 4 shows a hypothetical ave age weighted error curve for an anten This curve is obtained in the following manner. A chart is prepared showing the error measurements made at vari points on the surface of the reflector u consideration. A number of weighting tors are determined, which take into a the illumination amplitude at each of t points at which an error measurement made. The error values are then mul plied by the proper weighting factor, a a correction is made to compensate fo improper zero setting of the depth gag used to make the mechanical measure ments. The values of weighted error are then plotted to correspond to the horizontal (or distance along the antenna, and an average is taken at each value of x to give the average weighted curve. If this curve indicates that the reflector was slightly tilted when in the measuring jig, a further correction for tilt is applied. The final result will appear as sh in Figure 5. The derived curve shown is obtained by finding the algebraic difference bet the values of the average weighted error curve at corresponding positive and negative va of x. The derived curve is useful in analyzing the results for the effects on coma lobes a side lobes.

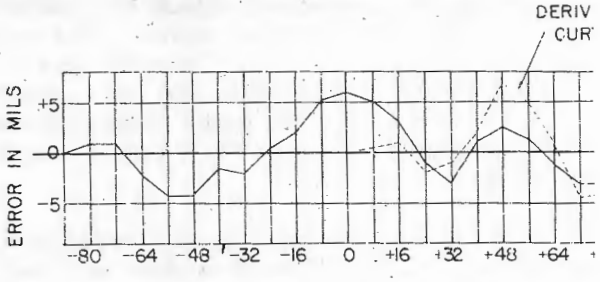

Figure 5 - A hypothetical average weighted error curve for an antenna

By comparing Figures 4 and 5, we may see what effect the mechanical errors in the reflector will have on its electrical characteristics. The chart indicates that the main beam will be narrower than would be expected from the design of the reflector, since a considerable error exists in the center region of the reflector. A consideration of the error distribution also shows that we may expect a fairly high side lobe. If the curve is examined for coma lobes and maximum swing, indications are that fairly good results will be obtained with t reflector. Thus, the critical characteristic of this reflector seems to be the side lobes, s that an electrical measurement should be made to determine the actual side-lobe power l

The method described has proved to be an important aid in obtaining considerable inf mation about each reflector before any electrical testing is performed. The correlation between theory and actual results has not been completely established.

In addition the method has been successful in establishing, in one type of antenna, the ratio of beam to dish tilt as a function of tilt axis position. The method has been used in a production run of a considerable number of reflectors, and it is felt that it may well be of value in the analysis of other types.

(This paper based on a Classified Hazeltine Electronics Corporation Report by F. W. Frink, under Contract NObsr-42428.)

* * *

An Antenna Pattern Synthesis Method

T. T. Taylor
Research and Development Laboratories
Hughes Aircraft Company

EDITOR'S NOTE:

During one of the discussion periods Mr. Taylor described briefly an analysis useful in relating the far-field radiation pattern to the corresponding aperture illumination. The pattern is shown to be obtained from a sum of sin x/x functions or from the product of a transcendental function and a polynomial. The following paper gives the details of this analysis.

An aperture distribution function g(x) which vanishes outside the interval $-a \leqslant x \leqslant a$ and which within that interval is expressible as a finite sum of N Fourier terms as follows

$$g(x) = \sum_{n=-N/2}^{N/2} A_n e^{-i\frac{n\pi x}{a}} \qquad (1)$$

will give rise to a pattern $S(\nu)$, where $\nu = \cos\alpha$, having the following characteristics:

1. $S(\nu)$ will have zeros at $\nu = \pm(\frac{N}{2}+1)\lambda/2a$,
$\pm(\frac{N}{2}+2)\lambda/2a, \pm(\frac{N}{2}+3)\lambda/2a, \ldots\ldots, \pm\infty\,\lambda/2a$.

2. In addition to this infinite set of equally spaced zeros on the real axis, $S(\nu)$ may have as many as N additional zeros placed anywhere in the complex z plane, where $z = \nu + i\sigma$.

In (1), N may be either even or odd; if the latter, then n is always an integer plus one-half. In any event, n changes by one integer in going from one term to the next. The angle α is the angle between the axis of the distribution and the direction of the observer.

THE SYNTHESIS METHOD OF WOODWARD

P. M. Woodward has described an ingenious synthesis method[1] which involves the use of a finite sum of functions of the form

$$\frac{A_n \sin ka(\nu - \nu_n)}{ka(\nu - \nu_n)}$$

to form the desired $S(\nu)$. The inverse transform of such a sum is clearly an acceptable g(x); the problem, therefore, is how to best set up this sum of functions. Let us say that

[1] Woodward, P. M., "A Method of Calculating the Field over a Plane Aperture Required to Produce a Given Polar Diagram," J. Inst. Elec. Engrs. (London), 93, Part IIIA, 1554 (1946)

N + 1 such functions will be used. These are displaced from one another by integral multiples of $\lambda/2a$ (one "beamwidth") which means that the principal maximum of each function coincides with a zero of all the others. We have, then, for the space factor:

$$S(\nu) = 2ka \sum_{n=-\frac{N}{2}}^{\frac{N}{2}} A_n \frac{\sin ka\left(\nu - \frac{n\lambda}{2a}\right)}{ka\left(\nu - \frac{n\lambda}{2a}\right)} . \tag{2}$$

If we adopt a new variable, w, which indicates numbers of beamwidths,

$$w = \frac{2a\nu}{\lambda} . \tag{3}$$

Equation 2 becomes:

$$S(w) = 2ka \sum_{n=-\frac{N}{2}}^{\frac{N}{2}} A_n \frac{\sin \pi (w - n)}{\pi (w - n)} . \tag{4}$$

The inverse transform g(x) is given by:

$$g(x) = \sum_{n=-\frac{N}{2}}^{\frac{N}{2}} A_n e^{-i\frac{n\pi x}{a}} \qquad x^2 \leqslant a^2$$

$$g(x) = 0 \qquad x^2 > a^2 \tag{5}$$

The technique advanced by Woodward for finding the A_n was simply that of demanding that S(w) pass through N + 1 points spaced by integers in w. Thus:

$$A_n = \frac{1}{2ka} \left[R(w)\right]_{w=n} . \tag{6}$$

This method is excellent for certain types of problems, but is not likely to lead to super-gain solutions involving high "invisible lobes" because, among other reasons, the person using the method will not know how to insert such lobes in the invisible region in order to achieve a desired effect in the visible region. The method also does not provide us with a means for approximating any given continuous and single-valued function R(w) arbitrarily exactly — a thing which we know we should be able to do. One of the reasons for this is that some R(w) functions cannot be adequately described by a set of values at points spaced by integers within the operating range. (Super-gain problems are of this type.) There are other cases also where, by the very nature of the problem, the values of R at points spaced by integers must remain unknown until a solution is obtained. Such is the case when one desires to find a continuous aperture distribution with minimum beamwidth for a given side-lobe level. Finally, we have the case wherein it is desired to approximate a real R(w) by $|S(w)|$, allowing the A_n to become complex. Woodward himself indicated that this would be the ultimate in generality, but said nothing about how such a thing could be realized. The method to be discussed in this paper is intended to extend Woodward's method in such a way as to accommodate these situtations which otherwise could not be readily handled.

ANALYSIS OF THE FUNCTION S(w)

We will attempt, in this section, to show that S(w) is expressible as the product of a transcendental function $Q_N(w)$ and a polynomial P(w). Thus, where K is a constant:

$$P(w) = \frac{S(w)}{KQ_N(w)} . \tag{7}$$

If this is true, the problem reduces to that of approximating the quotient $R(w)/KQ_N(w)$ by a polynomial, and all of the well-known techniques for synthesizing polynomials can com into play. The result is that the scope of Woodward's method is extended considerably.

Consider Equation 4 for N = 2, for example.

$$S(w) = 2ka \left[\frac{A_{-1} \sin \pi(w+1)}{\pi(w+1)} + \frac{A_0 \sin \pi w}{\pi w} + \frac{A_1 \sin \pi(w-1)}{\pi(w-1)} \right] . \tag{8}$$

This may be written:

$$S(w) = \frac{2ka \sin \pi w}{\pi^3} \left[\frac{-A_{-1}}{w+1} + \frac{A_0}{w} + \frac{-A_1}{w-1} \right] . \tag{9}$$

The bracketed quantity above is the partial fraction expansion of a rational function consisting of a polynomial of degree 2 divided by a polynomial of degree 3, the latter having roots at -1, 0, and +1. In other words we may write:

$$S(w) = \frac{2ka \sin \pi w}{\pi^3 (w+1)(w)(w-1)} \left[B_0 + B_1 w + B_2 w^2 \right] . \tag{10}$$

The transcendental function $\sin \pi w / \pi(w+1)(w)(w-1)$ is simply the sine function with three zeros divided out; it will be denoted $Q_2(w)$. The space factor for this case is evidently:

$$S(w) = \frac{2ka}{\pi^2} Q_2(w) P(w) . \tag{11}$$

An extension to higher orders yields the following general formulae: For N even:

$$Q_N(w) = \frac{(-1)^{\frac{N}{2}} \left(\frac{N}{2}!\right)^2 \sin \pi w}{\pi \left(w + \frac{N}{2}\right)\left(w + \frac{N-2}{2}\right) \cdots (w) \cdots \left(w - \frac{N-2}{2}\right)\left(w - \frac{N}{2}\right)} . \tag{12}$$

For N odd:

$$Q_N(w) = \frac{(-1)^{\frac{N+1}{2}} \left(\frac{N}{2}!\right)^2 \cos \pi w}{\pi \left(w + \frac{N}{2}\right)\left(w + \frac{N-2}{2}\right) \cdots \left(w + \frac{1}{2}\right)\left(w - \frac{1}{2}\right) \cdots \left(w - \frac{N-2}{2}\right)\left(w - \frac{N}{2}\right)} \tag{13}$$

For [2] any N:

$$Q_N(w) = \frac{\left(\frac{N}{2}!\right)^2}{\left(\frac{N}{2}+w\right)! \left(\frac{N}{2}-w\right)!} . \tag{14}$$

[2] See Jahnke, E., and Emde, F., "Tables of Functions with Formulae and Curves," New Y Dover (1945) P. 12

The functions $Q_N(w)$ form a most interesting class. They are entire transcendental functions, real for real argument. Each is actually either a sine or cosine of πw with the N+1 central zeros removed. At the points where the zeros have been removed, the functions attain values which are proportional to the coefficients in the binomial expansion of order N. Thus:

$$\left.\begin{aligned} Q_4(-2) &= 1/6 \\ Q_4(-1) &= 4/6 \\ Q_4(\ 0) &= 1 \\ Q_4(+1) &= 4/6 \\ Q_4(+2) &= 1/6 \end{aligned}\right\} \tag{15}$$

Finally, for high orders the approximation of Laplace is applicable:

$$Q_N(w) \simeq e^{-\frac{2w^2}{N}} \tag{16}$$

This indicates that the central section of the Q_N functions have the appearance of the normal distribution curve. Figure 1 shows the first four $Q_N(w)$, with the Laplace approximation for $Q_3(w)$ plotted for comparison.

To summarize, the general expression for the space factor becomes:

$$S(w) = \frac{2ka}{\pi N \left(\frac{N}{2}!\right)^2} Q_N(w)\, P(w) \ . \tag{17}$$

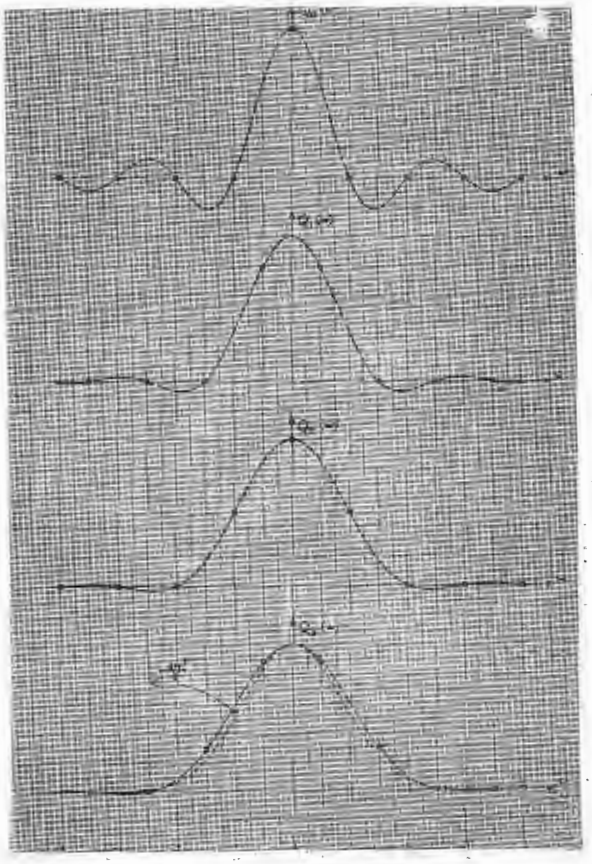

Figure 1 - First four $Q_N(w)$ curves with the Laplace approximation for $Q_3(w)$ plotted for comparison

* * *